Earth and Planetary Science Letters 601 (2023) 117906

Contents lists available at ScienceDirect

Earth and Planetary Science Letters

journal homepage: www.elsevier.com/locate/epsl

Retracing the Africa–Eurasia nascent convergent boundary in the western Mediterranean based on earthquake and GNSS data

Andrea Billi [a], Marco Cuffaro [a], Barbara Orecchio [b], Mimmo Palano [c], Debora Presti [b,*], Cristina Totaro [b]

[a] Consiglio Nazionale delle Ricerche, IGAG, Roma, Italy
[b] Department of Mathematics, Computer Sciences, Physics, and Earth Sciences, University of Messina, Messina, Italy
[c] Istituto Nazionale di Geofisica e Vulcanologia, Osservatorio Etneo – Sezione di Catania, Catania, Italy

ARTICLE INFO

Article history:
Received 5 September 2022
Received in revised form 31 October 2022
Accepted 4 November 2022
Available online xxxx
Editor: H. Thybo

Keywords:
seismicity
GNSS
seismogenic stress
crustal strain
plate convergence
western Mediterranean

ABSTRACT

In the western Mediterranean, following the intervening continent-continent collision, the subduction of the Tethyan ocean has progressively come to an end or almost in large sectors. Compressional deformation connected with the ongoing Africa–Eurasia convergence has therefore progressively resumed mostly along the southern passive margins of the Mediterranean back-arc basins. The aim of this paper is to trace this nascent boundary and constrain its kinematics through geodetic and seismological data recorded between the Ionian Sea and Gulf of Cadiz, and through pre-existing tectonic data. Based on these data, the nascent plate boundary is drawn, kinematically defined, and compared with the previously identified boundaries in the same region. The nascent boundary is weaving and formed by variably oriented inherited structures. It is characterized by a discrepancy between the general motion of Africa with respect to Eurasia and the local contractional/compressive axes deduced from geodetic and seismic data. The oblique convergence along the nascent boundary matches that recorded in other instances of subduction initiation elsewhere; however, the average convergence rate ($\sim$ 5 mm/yr) in the Mediterranean seems currently too small for such a subduction initiation. Based on the assumption of a future northward tectonic vergence (i.e., Eurasian foreland), the Tyrrhenian, Algerian, and Betic salients, the Oran and Fès recesses, and the Ionian, Trans-Alboran, and Gibraltar transfer zones are identified along the nascent boundary. The latter zones connect salients and recesses through strike-slip displacements. The Algerian offshore hosts a long segment of the boundary characterized by locally increased seismic rate and actual northward vergence that would suggest this area being the first nucleus of subduction initiation in the western Mediterranean, as was previously proposed.

1. Introduction

In what is now the western Mediterranean and adjacent areas, the Africa (i.e. the plate to the west of the East African Rift as reported in Kreemer et al., 2014, elsewhere termed Nubia) and Eurasia plates (AF and EU, respectively) have converged and interacted since at least the Paleogene time ($>$ 35 Ma; Faccenna et al., 2014 and references therein; Fig. 1). Convergence has led to subduction and consumption of old oceanic basins (Tethys) and related mountain building (e.g., Apennines, Maghrebides, Rif, and Betics). Within this framework, slab rollback has led to the development of at least two main (back-arc) basins, namely the younger Tyrrhenian basin toward the east and the older Liguro-Provençal basin elongating westward into the narrow Algerian and Alboran basins (van Hinsbergen et al., 2020 and references therein).

Subduction along the studied boundary (western Mediterranean) has progressively come to an end or almost in large sectors (e.g., Maghrebides slab break-off) due to intervening continent-continent collision. However, as the convergence between Africa and Eurasia is still ongoing, active compressional deformation is mostly being resumed from the old subduction-suture zones to the southern (and partly to the northern) passive margins of the aforementioned back-arc basins (i.e., the western Mediterranean), where tectonic inversion (from extension to compression) started diachronously from west to east: since about 8 Ma in the Alboran and Liguro-Provençal basins and since about 2 Ma in the Tyrrhenian basin (Jolivet and Faccenna, 2000; Meghraoui et al., 2004; Déverchère et al., 2005; Kherroubi et al., 2009; Billi et al., 2011; Lallemand and Arcay, 2021; Strzerzynski et al., 2021). Therefore, tectonic processes are presently heading toward the progressive

* Corresponding author.
E-mail address: dpresti@unime.it (D. Presti).

https://doi.org/10.1016/j.epsl.2022.117906
0012-821X/

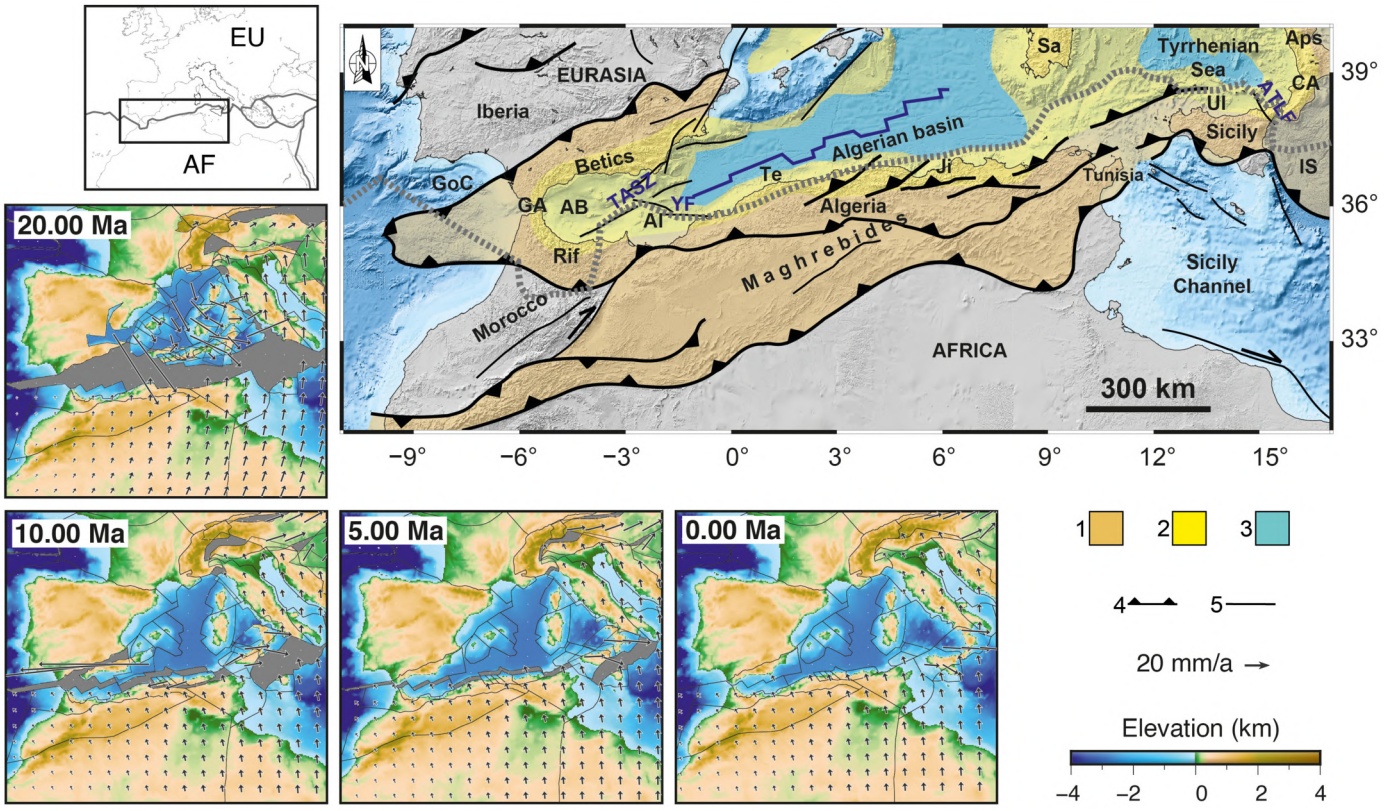

Fig. 1. Simplified tectonic map of the western Mediterranean area. Keys: 1 = post-orogenic basins, 2 = Neogene shortening, 3 = Neogene oceanic crust, 4 = main thrusts, 5 = generic faults. Abbreviations: AB = Alboran Basin; AF = Africa plate; AI = Alboran Island; Aps = Apennines; ATLF = Aeolian-Tindari-Letojanni fault system; CA = Calabrian Arc; EU = Eurasia plate; GA = Gibraltar Arc; GoC = Gulf of Cádiz; IS = Ionian Sea; Ji = Jijel; Sa = Sardinia (i.e., the southern sector of the Sardinia-Corsica continental block); TASZ = Trans-Alboran shear zone; Te = Ténès; UI = Ustica Island; YF = Yusuf fault system. The small panels (bottom and left sides) show the plate reconstructions of the western Mediterranean region during the last 20 Ma (see text for details). Africa plate and other microplate displacements and velocities were computed with respect to the fixed Eurasia plate, using the Gplates software (www.gplates.com), also including plate polygons (black solid lines) and relative plate vectors provided by Müller et al. (2019). (For interpretation of the colors in the figure(s), the reader is referred to the web version of this article.)

inversion and closure of the western Mediterranean basins, presumably through the development of a new convergent boundary (Déverchère et al., 2005; Billi et al., 2011; Auzemery et al., 2021; Leffondré et al., 2021; Strzerzynski et al., 2021; Thorwart et al., 2021; Klingelhoefer et al., 2022). Due to the nascent or immature (sensu Lallemand and Arcay, 2021) nature of this boundary, thrust faults are as yet far from developing into a convergent plate boundary and hence its geometric details are still only partially known as are the related kinematics and potential future evolution.

Studying and understanding plate convergent zones is societally relevant for the large earthquakes and related tsunamis that these zones can generate (e.g., Okal and Synolakis, 2008). This is particularly true for the western Mediterranean basin, where despite the not so frequent tsunami occurrence, the presence of active tsunamigenic faults can seriously threaten the densely urbanized coastal zones. In this paper, we reconsider the present tectonics of the western Mediterranean, i.e., between the western Ionian Sea and the Gulf of Cadiz (Fig. 1), to retrace the nascent AF-EU plate boundary using earthquake and GNSS data with the help of existing tectonic data. We then compare the newly drawn boundary with the ones drawn in the same region in the literature (DeMets et al., 1990, 2010; Bird, 2003), particularly with that of DeMets et al. (2010). In synthesis, main novelties of this work are the geodetic-seismic databases, particularly the new geodetic one derived from the ITRF14 reference frame (Altamimi et al., 2017), the newly drawn nascent plate boundary between Africa and Eurasia in the western Mediterranean, its kinematics and complex architecture, its comparison with previously drawn boundaries in the same region, and some broad tectonic implications.

2. Tectonic setting

The present-day tectonics of the study region (Fig. 1) is related to the Paleogene-Neogene tectonic evolution of the western Mediterranean subduction zones, which is mainly interpreted with a slab retreat model (Fig. 1; e.g., Carminati et al., 1998; Royden and Faccenna, 2018; Müller et al., 2019; van Hinsbergen et al., 2020; Jolivet et al., 2021; Haidar et al., 2022 and references therein). According to plate reconstructions (Fig. 1), accretionary wedges made of folds and thrusts grew migrating toward the foreland (mostly Africa but also Eurasia in some places) while the associated subduction zones retreated toward the same foreland and related back-arc basins formed on the hinterland side, i.e., at the rear of the accretionary wedge (Jolivet et al., 2021 and references therein). Consequently, at present, two main tectonic domains can be recognized in the western Mediterranean: the accretionary wedges made of folds and thrusts, and the back-arc basins (Fig. 1). The former includes the Apennines, Maghrebides, Rif, and Betics fold-thrust belts, whereas the latter includes the Tyrrhenian, Liguro-Provençal, Algerian, and Alboran basins (Kastens and Mascle, 1990; Sartori, 1990; Faccenna et al., 2014; Royden and Faccenna, 2018; Jolivet et al., 2021).

As mentioned above, contractional deformation is now occurring in the western Mediterranean basins, where back-arc compression and inversion started since about 8 Ma or even earlier in the west and propagated toward the east in the Tyrrhenian basin

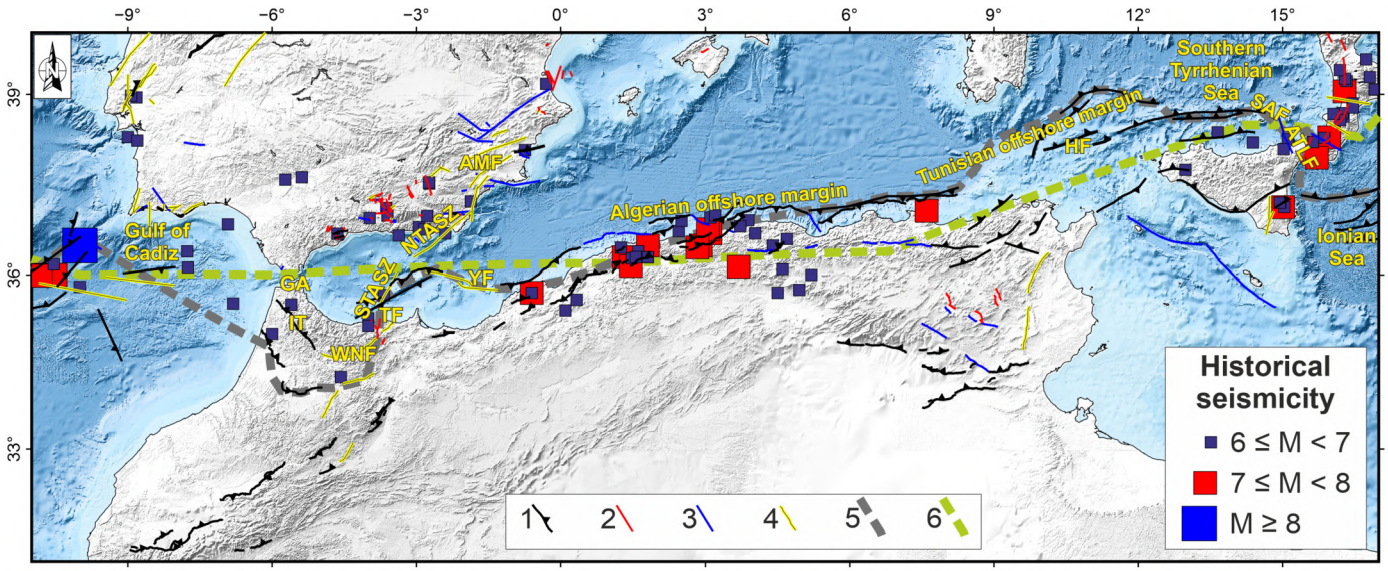

Fig. 2. Active faults (with documented Holocene activity) for the western Mediterranean compiled from recent literature (e.g., Palano et al., 2012, 2015; Echeverria et al., 2013; Gràcia et al., 2019) and online databases (https://github.com/GEMScienceTools/gem-global-active-faults; https://www.seismofaults.eu/efsm20draft). Keys: (1) reverse and/or thrust faults; (2) normal faults; (3) sinistral strike-slip faults; (4) dextral strike-slip faults; (5) Africa–Eurasia plate boundary defined in Bird (2003), which is the same boundary of DeMets et al. (2010); (6) Africa–Eurasia plate boundary defined in DeMets et al. (1990). Historical earthquakes of the study area in the last millennium ($M \geq 6.0$) are also reported as squares (see Table S1 for details). Abbreviations are as following: GA, Gibraltar Arc; IT, Internal thrust; WNF, western Nekor fault; TF, Trougout fault system; STASZ, southern Trans-Alboran shear zone; NTASZ, northern Trans-Alboran shear zone; YF, Yusuf fault system; AMF, Alhama de Murcia fault system; HF, Hatay fault; SAF, Sisifo-Alicudi fault system; ATLF, Aeolian-Tindari-Letojanni fault system.

(Carminati et al., 1998; Wortel and Spakman, 2000; Faccenna et al., 2014), leading Billi et al. (2011) to hypothesize the initiation of a new scissor-like (i.e., progressing from west to east in a scissor-like manner) subduction system along the passive margins of the western Mediterranean basins. Indeed, nascent subduction zones in the western Mediterranean, particularly off Algeria, had already been proposed by many studies (e.g., Meghraoui et al., 2004; Déverchère et al., 2005; Kherroubi et al., 2009; Yelles et al., 2009). The precise location of this nascent plate boundary, from the western Ionian Sea to Gibraltar and over in the Gulf of Cadiz, is still under debate due to the complexity of the crustal deformation, to fault locking over long seismic cycles, and to the nascent and changing nature of the boundary itself (e.g., Serpelloni et al., 2007; Zitellini et al., 2009; Jolivet et al., 2021; Lallemand and Arcay, 2021).

At least three main attempts of identifying and drawing the AF-EU nascent boundary over the entire western Mediterranean have been so far attempted (DeMets et al., 1990, 2010; Bird, 2003). Since 1990, the NUVEL-1 AF-EU boundary (Fig. 2) in the Mediterranean region (DeMets et al., 1990) has been extensively used for plate kinematic applications and strain and stress field evaluations (e.g., Serpelloni et al., 2007 and references therein). After about a decade, Bird (2003), based on multidisciplinary data, proposed a new global collection of digital plate boundaries (including the western Mediterranean) and Euler vectors. Substantial differences can be observed between the AF-EU boundaries proposed in 1990 and 2003 for the Mediterranean region (Fig. 2), especially for the segments located in the Gulf of Cadiz and Calabrian-Ionian Sea regions. The AF-EU boundary proposed by Bird (2003) is, in general, more articulated with respect to the one provided by DeMets et al. (1990) and located at lower latitudes in the Gulf of Cadiz, Gibraltar and Calabrian arcs, and at higher ones from Algeria to the Tyrrhenian Sea (Fig. 2). Eventually, the plate boundary proposed by DeMets et al. (2010) substantially coincides with that of Bird (2003), at least for the western Mediterranean.

The nascent boundary in the western Mediterranean includes active fault segments that are characterized by a large variety of orientation and kinematics (Fig. 2). Most of these faults are thrusts, highlighting the overall convergent nature of the AF-EU plate boundary in the western Mediterranean. Active thrusts mapped along the external orogenic belt show lengths of 20–80 km with orientations that follow the undulations of the orogenic margin and a prevalent southward vergence (Fig. 2); however, thrusts located on the northern Algeria offshore are characterized by lengths up to 160 km and prevalent northward vergence (Meghraoui et al., 2004), whereas thrusts and reverse faults located in northern Sicily and along its northern offshore seem mostly characterized by a general southward vergence (Billi et al., 2007 and references therein). Strike-slip faults concentrate in portions of the western Mediterranean such as in the Ionian Sea or the central and eastern sectors of the Alboran basin. Here, with a prevalent left-lateral kinematics, they define the NE-SW-oriented Trans-Alboran shear zone and the NW-SE-oriented Yusuf fault system (Echeverria et al., 2013; Gràcia et al., 2019; Fig. 2). Strike-slip faults occur also in south-eastern Iberia, in northern Algeria, in central Tunisia, NE Sicily, and western Ionian Sea (Palano et al., 2015; Polonia et al., 2016; Soumaya et al., 2018). Normal faults occur in central Betics, Tunisia, Sicily, and Calabria, and are generally characterized by limited lengths (10–50 km; Fig. 2) (Palano et al., 2012, 2015).

Ongoing activity and seismic behavior of faults in the western Mediterranean are documented by the occurrence of large historical and instrumental earthquakes (several $M \geq 6.0$ earthquakes), with the strongest ones of the last millennium (see Table S1 and Fig. 2) concentrating along northern Algeria (contractional kinematics) and southern Calabria (extensional kinematics) (Yelles-Chaouche et al., 2017; Gutscher et al., 2017).

3. Materials and methods

To analyze the seismic activity of the western Mediterranean, we selected, from the International Seismological Centre bulletin (Fig. 3a and Table S2), hypocentral locations of earthquakes with magnitude $M \geq 4.5$ and depth ≤ 40 km occurred between January 1904 and May 2021. From these data, by using the approach of Jiménez-Munt et al. (2003), we computed the seismic strain-rate distribution (Fig. 3b). Following the same earthquake selection criteria (i.e., $M \geq 4.5$, depth ≤ 40 km), we built a database of

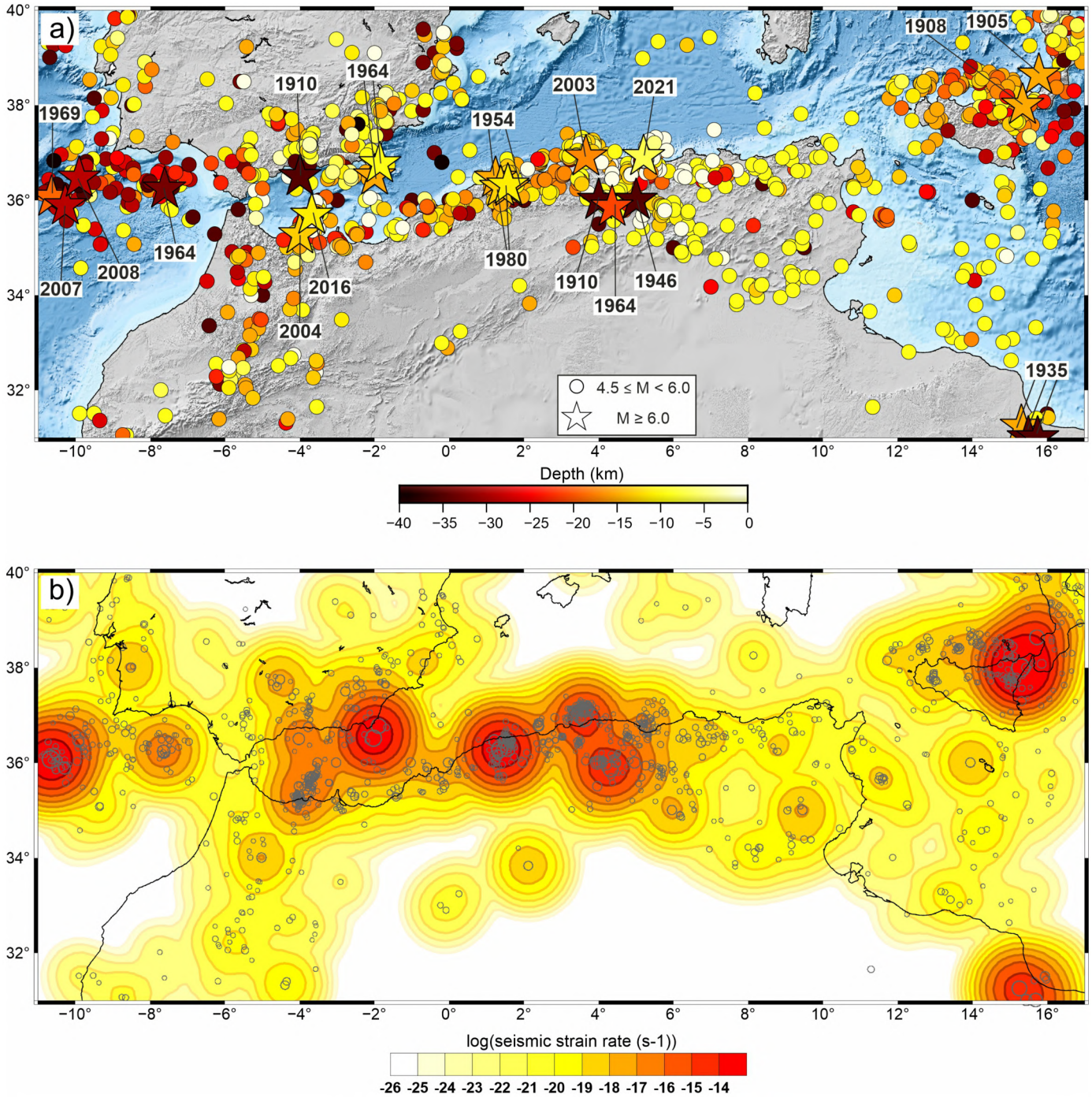

Fig. 3. (a) Map of earthquakes (i.e., epicenters) occurred in the study region (January 1904–May 2021, M ≥ 4.5) in the 0–40 km depth interval. Colors are for different focal depths (see legend). Data source: ISC bulletin (http://www.isc.ac.uk/iscbulletin/search/bulletin, Table S2). Earthquakes with M greater than or equal to 6 are labeled. (b) Seismic strain rate computed by using the approach of Jiménez-Munt et al. (2003, see Supplementary material). Earthquake data of plot (a) are reported as gray circles.

waveform inversion focal mechanisms (WIFMs hereinafter). This approach is widely recognized as much more powerful than first-motion inversion to elaborate focal mechanisms, especially in offshore regions, as happens for most of our study area (Presti et al., 2013). For this purpose, we integrated solutions from Centroid Moment Tensor catalogs (Global, gCMT; European-Mediterranean Regional, RCMT) and from the literature (Fig. 4, Table S3 and references therein), also including earthquakes occurred before the digital era (a period not fully covered by catalogs) and estimated by advanced techniques properly calibrated to work with analog data.

Starting from the above described datasets, we identified the main seismic sequences recorded from the western Ionian Sea to the Gulf of Cadiz (Fig. 5), by selecting those ones including at least one M ≥ 5.5 earthquake and no less than 5 events in our database (M ≥ 4.5). Due to the low number of seismographs operating during the early instrumental epoch and their poor capability of detecting aftershocks, we have a more complete set of seismic sequences in the western Mediterranean starting from the onset of the second half of the last century.

We used the collected WIFMs to estimate the seismogenic stress fields (Table S4), by applying the Bayesian algorithm of Arnold and Townend (2007). Such method furnishes the posterior

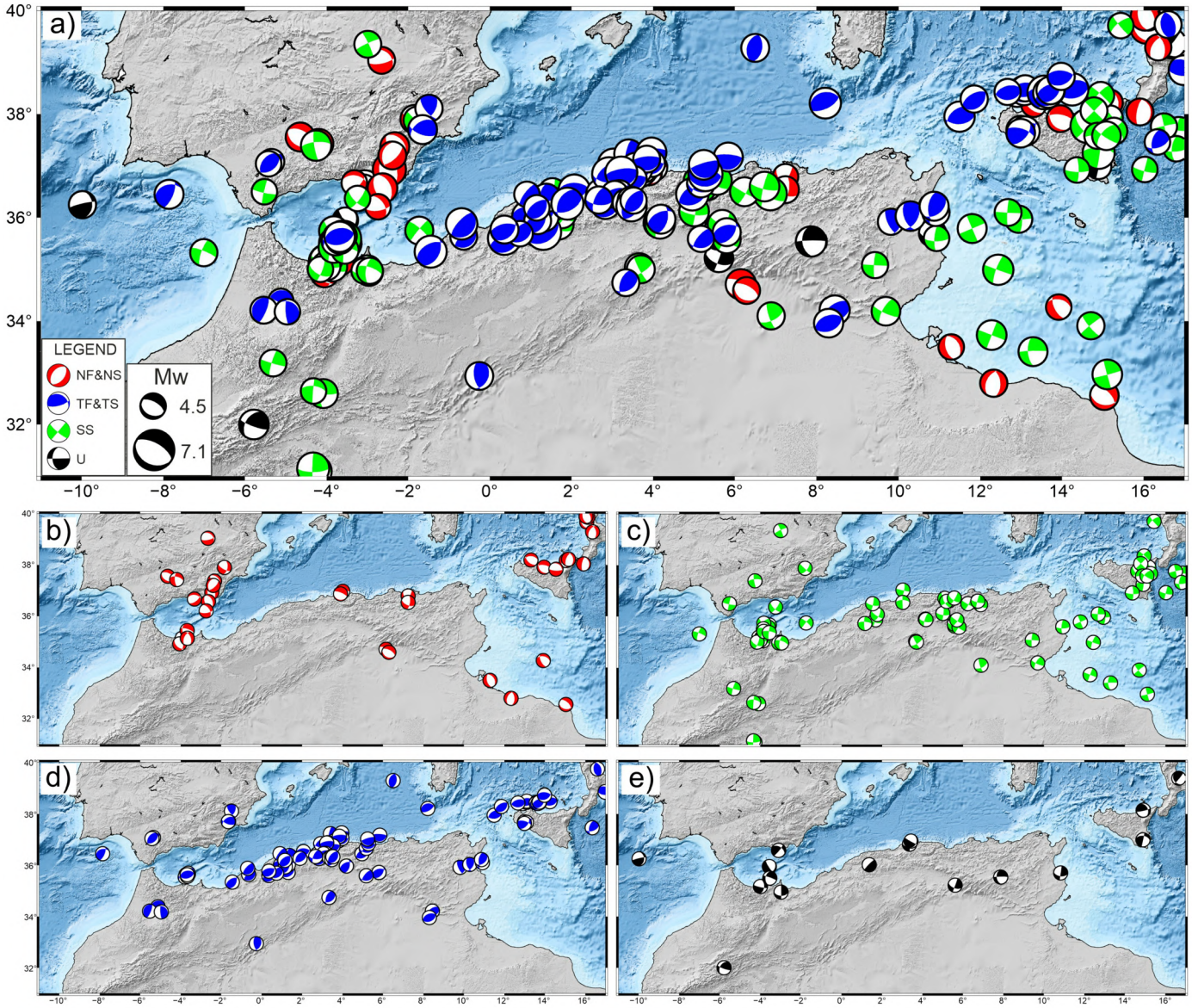

Fig. 4. (a) Distribution of waveform inversion earthquake focal mechanisms (depth range 0–40 km) for the western Mediterranean region collected from the gCMT (since 1976, https://www.globalcmt.org/CMTsearch.html) and the RCMT (since 1997, http://rcmt2.bo.ingv.it/) catalogs and from literature (see references in Table S3). Following the classification adopted in the World Stress Map (http://dc-app3-14.gfz-potsdam.de/), different colors identify different faulting types: (b) red = normal faulting (NF) and normal strike (NS); (c) green = strike-slip faulting (SS); (d) blue = thrust faulting (TF) and thrust strike (TS); (e) black = unknown stress regime (U). The beach ball size is proportional to the earthquake magnitude (see legend).

density function of the principal components of the stress tensor and the stress-magnitude ratio. To identify homogeneous subdomains for stress field computation (Fig. 6, see also Supplementary material), WIFMs were spatially grouped by evaluating their coherency and considering the plate polygon representation (Fig. 1) by Müller et al. (2019).

To analyze the crustal deformation pattern over the study region, we provided an original solution that is part of a continental-scale geodetic analysis of more than 2500 continuous GNSS stations operated by several local institutions, agencies, universities, and research institutes. We processed the GNSS raw observations by using the GAMIT/GLOBK 10.71 software package (http://www-gpsg.mit.edu) and adopting the methodology described in the Supplementary Material. Results of this processing consist of a set of positions and long-term velocities aligned to an Eurasia reference frame (Altamimi et al., 2017). To improve the spatial density of the geodetic velocity field over the study area, especially along northern Africa, we integrated our solutions with those reported in the recent literature (see Table S5), by solving for Helmert transformation parameters that minimize the differences between velocities at common sites. The final velocity field is reported in Fig. 7a and Table S5. This solution provides an improved picture of the horizontal crustal deformation of the study area since it is denser than the Mediterranean-scale solutions reported in recent literature (e.g., Nocquet, 2012; Devoti et al., 2017) and covers the Algerian and Tunisian regions, for which the previous crustal deformation pattern was deduced only on the basis of geodetic plate motion models (e.g., Kreemer et al., 2014). To provide additional insights into the present kinematics of the study area, we also estimated the horizontal strain-rates according to Shen et al. (2015). Due to varying station densities over the study area, we estimated the strain-rate field over a $0.75° \times 0.75°$ grid (see supplementary material) therefore resulting in a very smoothed pattern, which, however, well captures the main features of the investigated region (Fig. 7b).

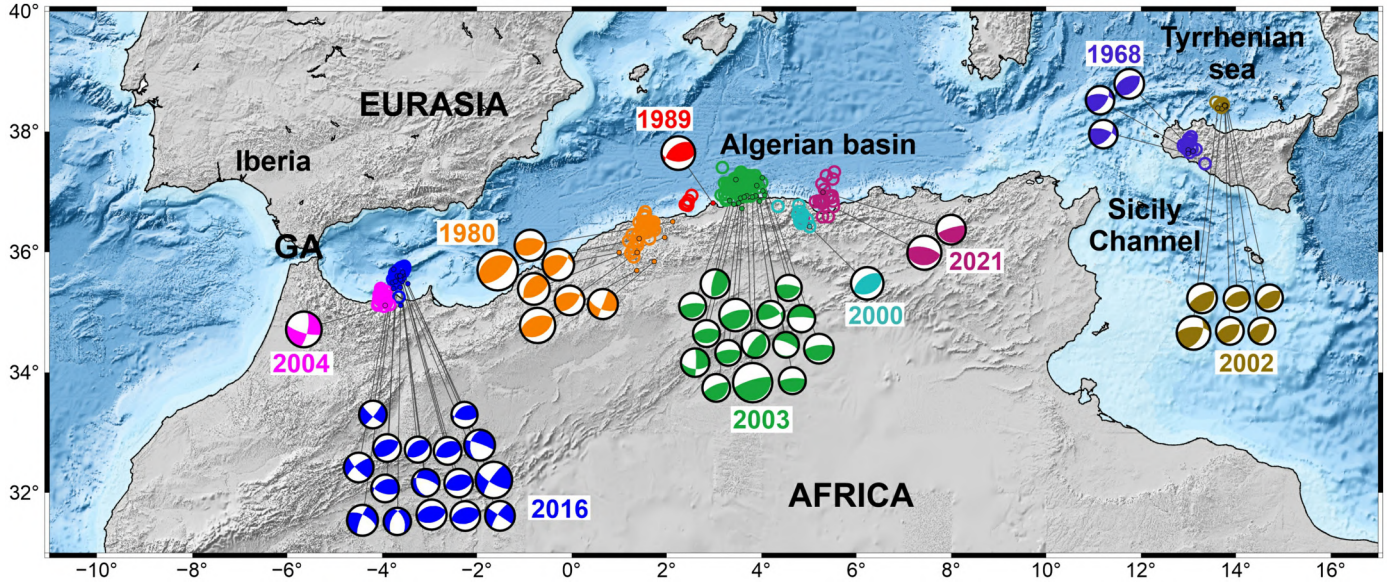

Fig. 5. Main seismic sequences that occurred in the western Mediterranean since about 1950 (see section 4.1 for details). Earthquake epicenters (data from Table S2) for each seismic sequence are reported with circles of different colors together with the year of occurrence. WIFMs (data from Table S3) associated to each sequence are also shown.

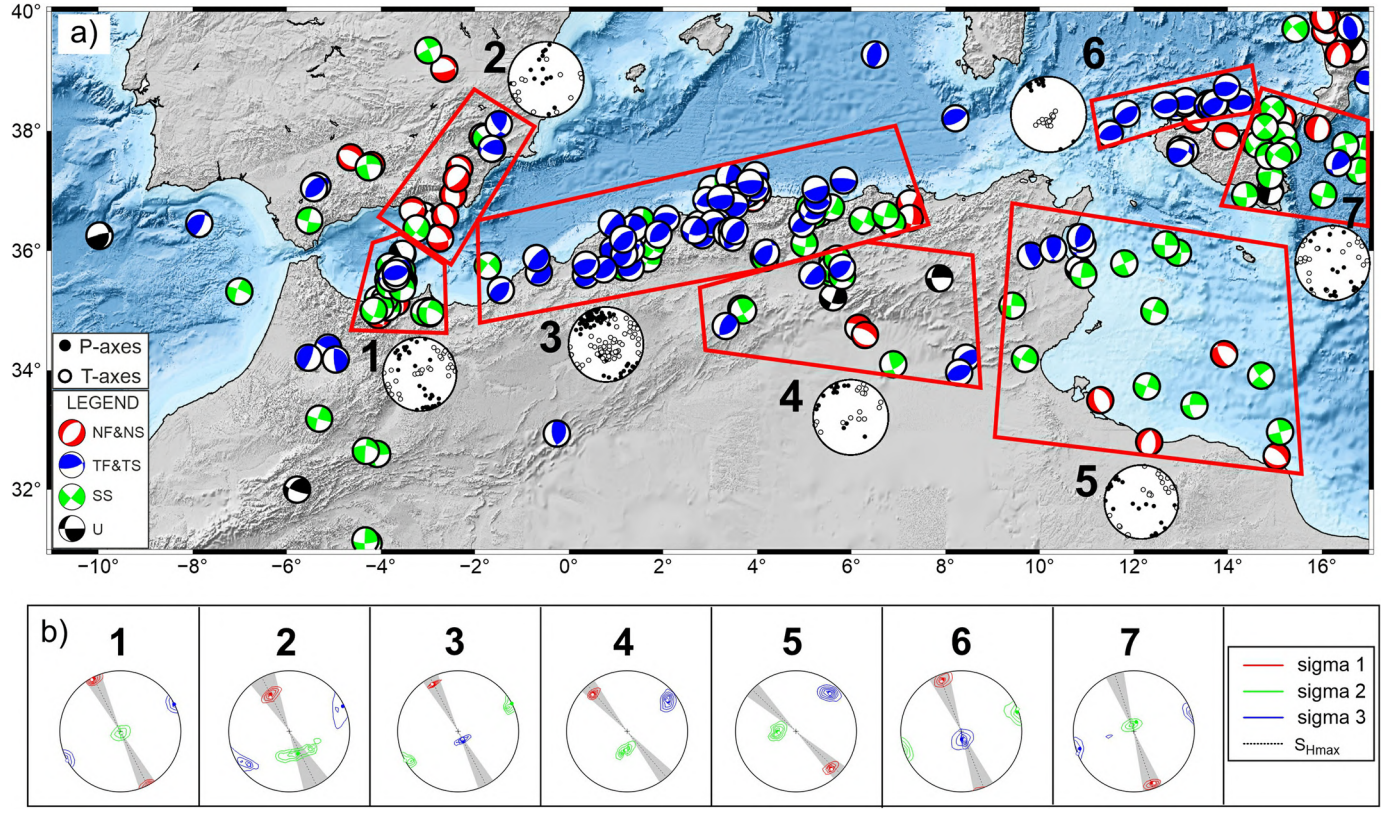

Fig. 6. (a) Polar plots of P- and T-axes (displayed with the standard representation: black = P and white = T) from focal mechanisms grouped in different domains (red polygons in map) defined starting from the model by Müller et al. (2019) and the WIFMs coherency. (b) Stereonets show the orientations of the principal stress axes estimated for each subset by applying the method by Arnold and Townend (2007; lower hemisphere projection; north is up, east is right). In the plots, the attitude of the σ_1, σ_2, and σ_3 axes are displayed as red, green and blue contours, respectively. The orientation of S_{Hmax} is also reported as a black dashed line with the 68% confidence intervals shaded in gray.

Tectonic data, i.e., mainly regarding location of main active faults with related kinematics (Fig. 2, Table 1), have been collected from recent literature (e.g., Billi et al., 2011; Cuffaro et al., 2011; Palano et al., 2012, 2015; Polonia et al., 2016; Gutscher et al., 2017; Echeverria et al., 2013; Gómez de la Peña et al., 2018, 2022; Gràcia et al., 2019; Strzerzynski et al., 2021; Camafort et al., 2022; Klingelhoefer et al., 2022) and online databases (https://github.com/GEMScienceTools/gem-global-active-faults; https://www.seismofaults.eu/efsm20draft). Complete geodetic, seismological, and tectonic datasets together with further information about the used methods are in the Supplementary Material.

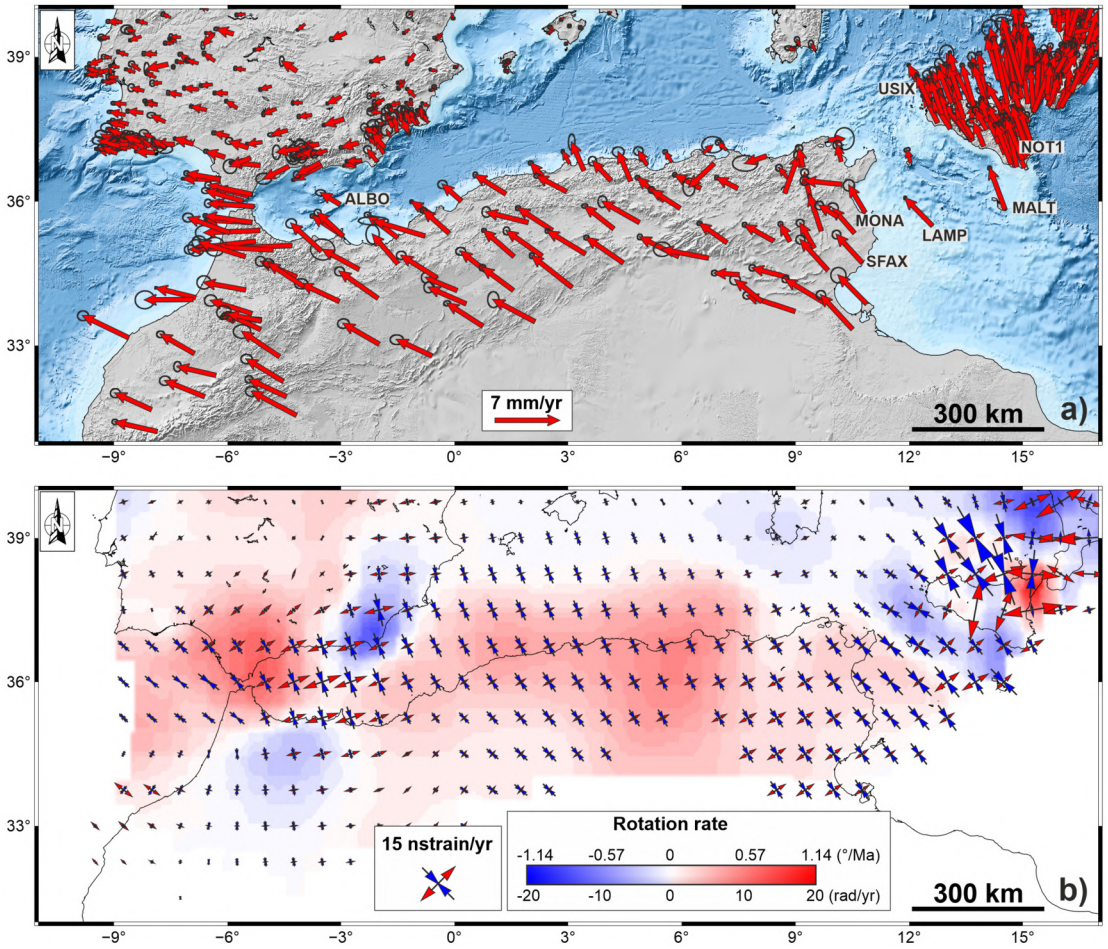

Fig. 7. (a) GNSS velocity field and associated 95% uncertainties referred to a fixed Eurasia reference frame. (b) Smoothed horizontal strain-rate field. The background color represents the rotation-rate describing the rotations with respect to a downward positive vertical axis with clockwise positive (red) and counterclockwise negative (blue), as in normal geological conventions, while arrows stand for principal strains (red for extension and blue for contraction).

4. Results and discussion

4.1. Crustal deformation

Our extensive seismic and geodetic datasets (Tables S1–S3 and S5) provide an improved picture of the current geodynamic setting of the western Mediterranean (Figs. 3–7), where the AF and EU plates are converging and interacting along a nascent convergent boundary (Fig. 8). Seismicity as well as the associated deformation is not homogeneously distributed across the new convergence zone. Most recorded seismicity is diffusely distributed over wide regions only in the Betics-Gibraltar-Rif, Tunisia, Sicily Channel, and Sicily (Figs. 3 and 4). Conversely, seismicity is concentrated along narrow WSW-ENE striking reverse regional-scale structures in northern Algeria, southern Tyrrhenian, and the easternmost Atlantic Ocean segment (Fig. 3), highlighting the current prevalent activity of these structures along the nascent boundary. In terms of seismic strain-rate pattern, relevant values can be observed for the easternmost Atlantic Ocean segment, Trans-Alboran shear zone, northern Algeria and eastern Sicily areas, while low values are found in the Gibraltar Arc and from eastern Algeria to western Sicily (Fig. 3).

WIFMs also depict a complex faulting pattern across the convergence zone, especially in the Betics and eastern Sicily, where a coexistence of reverse, normal, and strike-slip solutions occurs within a general framework of converging plates (Fig. 4a). Normal faulting activity mainly characterizes the Calabrian-Ionian region (Fig. 4b). Strike-slip solutions are relevant in northern Morocco-Alboran basin, in the internal sector of Algeria, and in the Sicily Channel (Fig. 4c), while a predominance of reverse solutions is visible in northern Algeria and south Tyrrhenian (Fig. 4d), where thrust faulting mechanisms mainly occur on E-to-NE striking fault planes.

Fig. 5 shows that significant seismic sequences occurred in Morocco, Algeria, Sicily and their northern off-shore areas (e.g., Bounif et al., 2004; Billi et al., 2007; Ousadou and Bezzeghoud, 2019; Orecchio et al., 2021). In particular, the most recent and energetic compressional seismic sequences (Fig. 5) are concentrated along the northern Algerian margin between Ténès (west) and Jijel (east), also corresponding with the largest seismic strain-rate in the investigated area (Fig. 3b). This seismicity, which occurred from 1980 to 2021 along different adjacent fault segments, confirms the pattern of historical earthquakes (Fig. 2). At least part of these earthquakes occurred along south-dipping thrust faults (i.e., northward tectonic vergence; e.g., Déverchère et al., 2005; Kherroubi et al., 2009; Yelles et al., 2009). Further significant seismic sequences occurred in the southern portion of the Trans-Alboran shear zone, but with strike- or oblique-slip kinematics (Fig. 5). Compressional seismic sequences (with magnitude smaller than those occurred along the Algerian margin) occurred in Sicily and off northern Sicily too (Fig. 5), where, however, the thrust vergence should be toward the south (Billi et al., 2007), hence implying a (re)activation/rejuvenation of the south-verging thrusts both at the front (1968 Belice M 5.5 earthquake) and at the rear (2002 south Tyrrhenian M 5.8 earthquake) of the fold-thrust belt (Billi et al., 2007, 2011). For other two sequences of comparable magnitude

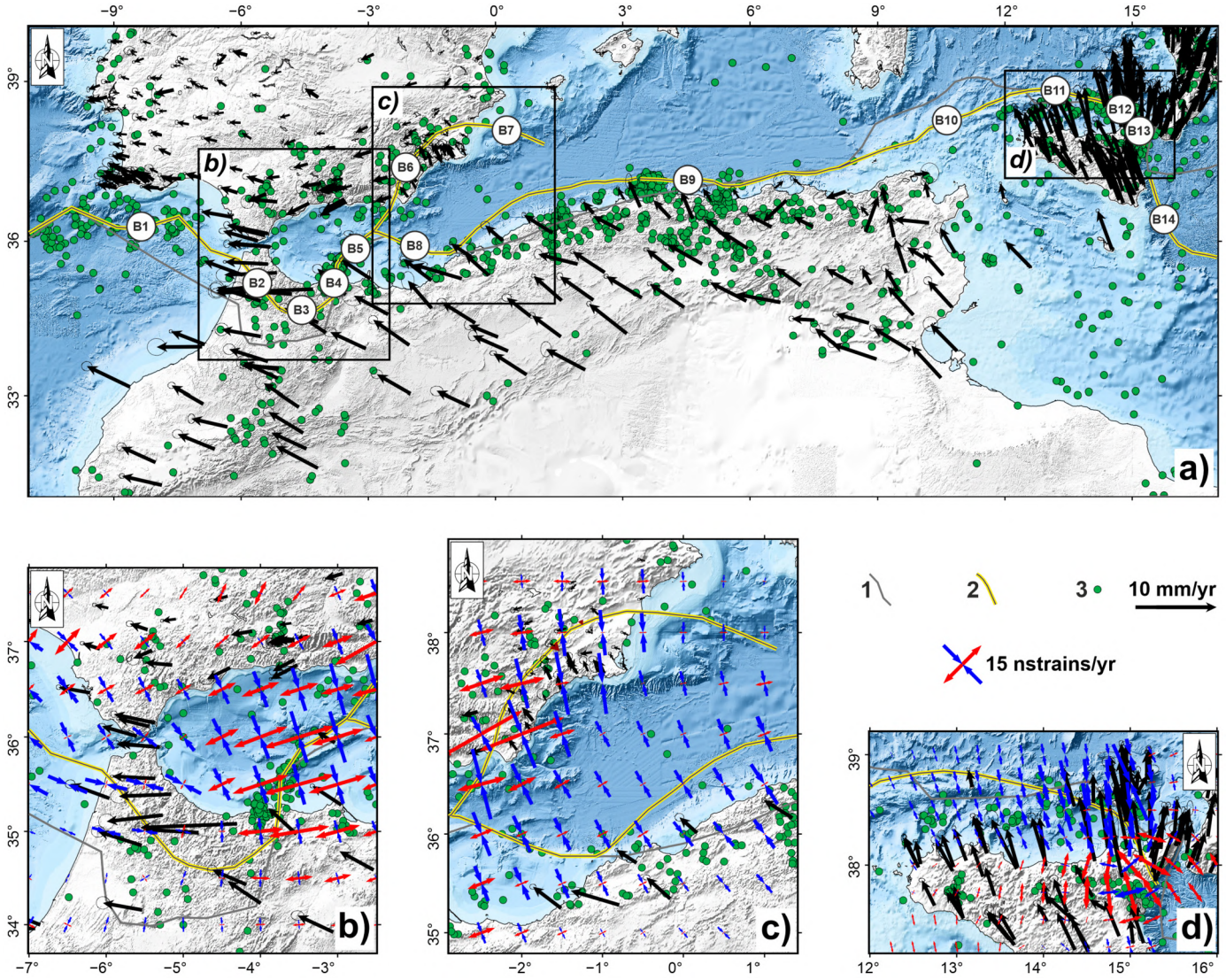

Fig. 8. (a) Overview of the nascent AF-EU plate boundary discussed in this study (Ionian Sea to Gulf of Cadiz). The previous boundary as identified in DeMets et al. (2010) is also reported. The nascent boundary has been primarily traced on the basis of our geodetic dataset and secondarily by taking into account information coming from our seismic dataset along with morpho-tectonic evidence and literature. Reverse or strike-slip kinematics have been inferred from the analyzed datasets. Instrumental $M \geq 4.5$ crustal seismicity along with GNSS velocity and strain-rate fields are also reported. Close-ups show: (b) western Alboran basin; (c) northwestern Algeria-southeastern Betics; and (d) northern Sicily-Tyrrhenian basin. Symbols are as follows: (1) plate boundary as identified in this study; (2) Africa–Eurasia plate boundary identified in Bird (2003), which is the same boundary of DeMets et al. (2010); (3) earthquakes. B1 to B14 are segments into which the AF-EU boundary identified in this work has been split up for descriptive reasons (see text).

(i.e., 1954, northern Algeria; 1969, western Gulf of Cadiz), only focal mechanism solutions computed from P-arrivals are available (McKenzie, 1972; Buforn et al., 2020) and, for this reason, they are not reported in Fig. 5; however, these latter solutions show reverse faulting with nearly-horizontal P-axes approximately oriented in the NW direction.

P/T axes distribution and estimated crustal seismogenic stress (Fig. 6, Fig. S1, Fig. S2, Table S4) provide clear evidence of a prevalent NW-trending active compression along the whole orogenic zone (Fig. 3). In particular, the northern Algeria and south Tyrrhenian areas (Sectors 3, 6, Fig. 6) are characterized by a well-defined NW-trending compressive stress regime. The Betics area (Sector 2, Fig. 6) appears to be less constrained with respect to the others, probably due to the high heterogeneity of the focal solutions. The remaining sectors (1, 4, 5, 7, Fig. 6) indicate mainly transcurrent tectonic regimes. Among these, the internal sectors of Algeria, Tunisia and Sicily channel (Sectors 4, 5, Fig. 6), including sparse earthquakes distributed on a wide region, show a slight counterclockwise rotation of the maximum compression axis with respect to other sectors (i.e. 3 and 6), further testifying their higher heterogeneity.

Additional evidence on the kinematic complexity of the study area (e.g., Nijholt et al., 2018) is provided by the GNSS data (Fig. 7). A primary feature of the geodetic velocity field is the NW-directed convergence of Africa with respect to Eurasia at rates of ~ 5 mm/yr. In Southern Italy, the geodetic velocity field (Fig. 7a) is characterized by a fan-shaped pattern passing from NNE-directed motion in Calabria and NE Sicily to a NNW-directed one in central-western Sicily, resulting in a general counterclockwise rotation with rates (Fig. 7b) up to 1.1 °/Ma (projected to geological timescales). A crustal extension up to 40 nanostrain/yr (Fig. 7b) with extensional axes oriented orthogonally to the curvature of the orogenic arc characterizes both Calabria and Sicily inland while the Sicilian offshore shows a contractional pattern with shortening axes up to 25 nanostrain/yr and with a prevailing NW-SE orientation. Stations located in southern Sicily (e.g., NOT1) and in the eastern Sicily Channel (MALT) show a slight divergence with respect to the ones located in the western Sicily Channel

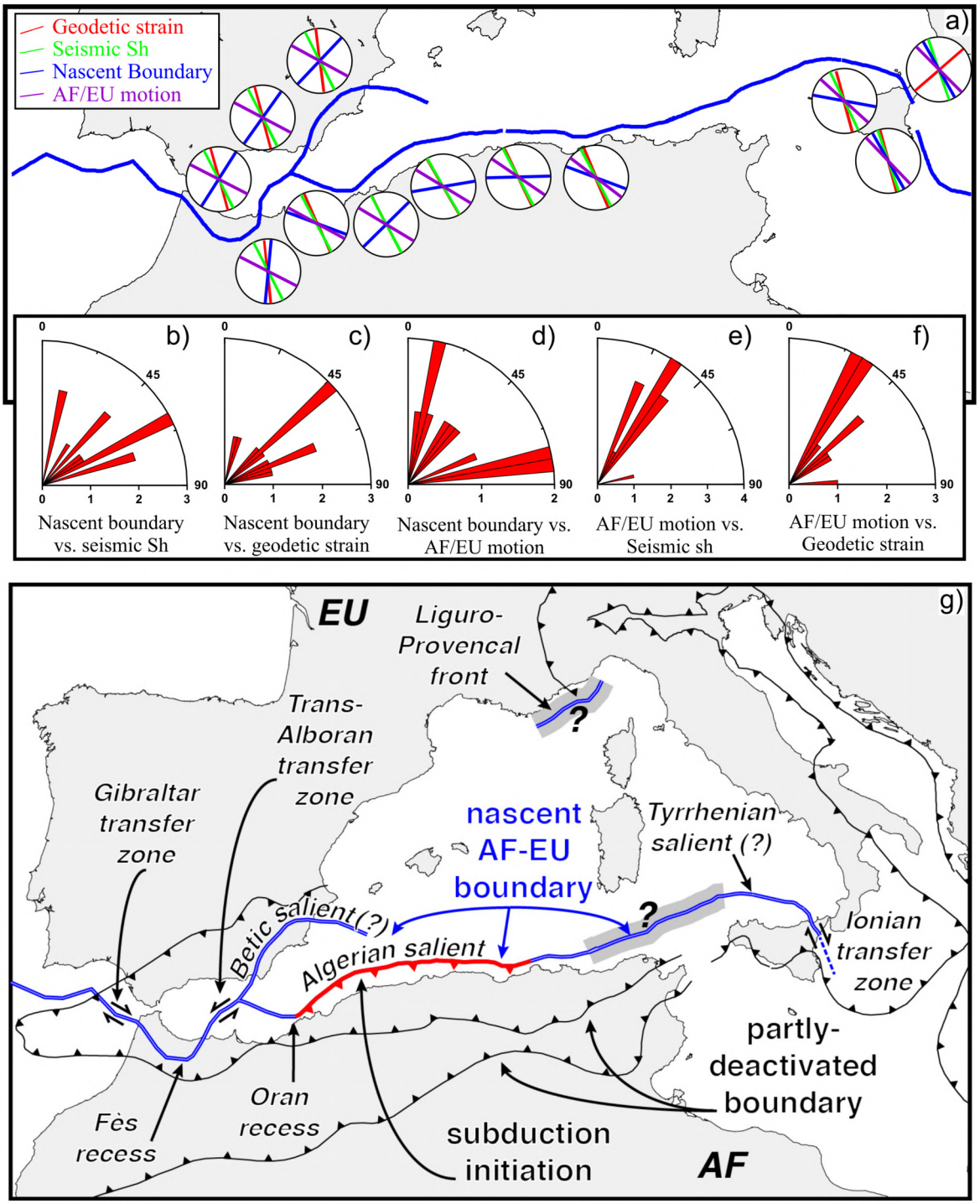

Fig. 9. (a) Simplified view of the angular relationships between the newly defined nascent boundary, the general motion of Africa with respect to Eurasia (computed according to Altamimi et al., 2017) and the horizontal components of compressive seismic stress (from Fig. 6) and geodetic strain (from Fig. 7). (b–c–d) Rose diagrams furnishing a cumulative picture of the angles that the nascent boundary forms with the maximum horizontal seismic stress axes Sh (b), geodetic strain-rates (c), and the general AF-EU motion (d); (e–f) Rose diagrams comparing the orientation of the general AF-EU motion with the seismic Sh (e) and geodetic strain-rates (f). (g) Sketch showing the complexity of crustal deformation along the nascent AF-EU boundary. In the central part of the area, a northward shift of the AF-EU boundary (blue line) is proposed, with respect to the pristine partly-deactivated boundary. In the assumption that Eurasia will be the future foreland, the nascent boundary in the western Mediterranean (blue boundary) is characterized by salients and recesses (convex-to-the-foreland and concave-to-the-foreland curves, respectively): i.e., the Tyrrhenian, Algerian, and Betic salients, and the Oran and Fès recesses. Transfer zones can be detected at the limbs of salients and recesses, with right-lateral kinematics in the Ionian and Gibraltar areas and left-lateral along the Trans-Alboran zone. Segments with high uncertainty (gray shadow) are observed between Tunisia and Sicily (to the south of Sardinia). As proposed previously (e.g., Billi et al., 2011 and references therein), part of the contractional displacement may be transferred from the southern Sardinia offshore to the Liguro-Provencal offshore, where compressional earthquakes occur (Bigot-Cormier et al., 2004). In the Algerian offshore (red segment), subduction initiation could occur as proposed by many studies (Lallemand and Arcay, 2021 and references therein). Question marks indicate questionable structures (see text).

(LAMP) and Tunisia (e.g., MONA, SFAX), confirming the different motion of this sector of the central Mediterranean Sea with respect to the large-scale motion of the Africa plate (Figs. 7 and 8; Palano et al., 2012). A significant northward velocity decrease is observed for Tunisia and eastern Algeria, with values of 5–6 mm/yr and 2–3 mm/yr at the southernmost stations and at the stations

located along the northern coastal area, respectively. Such a velocity gradient results in a contractional pattern with NW-SE-oriented shortening axes up to 10 nanostrain/yr, coupled with clockwise rotations with rates in the 0.17–0.57 °/Ma range (Fig. 7b). In western Algeria, the northward decrease of velocity values is less evident. This evidence, coupled with the NW-to-NE fan-shaped motion of southeastern Betics (counterclockwise rotations up to 0.86 °/Ma), highlights that part of the Africa–Eurasia convergence is also accommodated by on-land structures and suggests the existence of an independent crustal block in this sector of the Algerian basin (Figs. 7–9). In details, all stations show a similar azimuthal pattern with rates decreasing along the diffuse array of the left- and right-lateral strike-slip and reverse faults, belonging to the Trans-Alboran and Eastern Betics shear zones (see Echeverria et al., 2013 and Gómez de la Peña et al., 2022 for additional details). Therefore, the independent block lies in the offshore area in between the Eastern Betics and the Algerian margin and acts as a tectonic indenter as previously suggested by Palano et al. (2015). The Alboran basin is currently subject to NNW-SSE to N-S contraction at a rate of ∼ 3 mm/yr, as indicated by the stations located along the southern Betics and north-eastern Rif. ALBO station, for instance, shows a motion that is azimuthally coherent with the motion of the Africa plate. This feature, coupled with the low convergence rate (∼ 3 mm/yr), highlights that most of the oblique convergence is being accommodated along the Alboran Ridge fault system and the Trans-Alboran shear zone (Fig. 7a). In addition, the differential motion of the stations located on the northern-central Rif with respect to the ones located along the southern Betics highlights a clockwise rotation of the western sector of the Alboran basin up to 0.86 °/Ma, as clearly depicted by the rotational strain pattern reported in Fig. 7b. Stations located in the central sector of the Gibraltar Arc are characterized by a westward motion, leading to a small E-W stretching of the western side of the Alboran basin. Another relevant feature is the large-scale clockwise rotation of southern and western Iberia with respect to stable Eurasia, previously interpreted as a quasi-continuous strain of a large-scale ductile lithosphere (Palano et al., 2015).

4.2. The nascent AF-EU boundary

In the study area, we have drawn the nascent AF-EU plate boundary (Fig. 8) using our geodetic dataset – i.e., by analyzing both azimuthal and rate patterns – and, especially for regions not covered by GNSS stations, all pieces of information coming from our seismic dataset along with morpho-geo-structural data coming from the literature (Table 1 and Supplementary Material). For ease of description, we have analyzed and split up the nascent boundary in 14 sectors between the Gulf of Cadiz and the Ionian Sea (Fig. 8, Table 1). We have also compared our boundary with that previously proposed by DeMets et al. (2010) and have inferred plate kinematics along segments of the new boundary from GNSS data or by analyzing AF-EU velocities derived by the angular vectors of Altamimi et al. (2017), when no other data were available (Fig. S3). We acknowledge that, in many sectors, the line drawn by us as the nascent plate boundary may be an oversimplification of the present deformation that is possibly partitioned over a larger number of structures, each accommodating a small percentage of convergence (e.g., Camafort et al., 2022); however, we have no new tectonic data (active faults) to draw a diffuse boundary nor is this our goal. Moreover, the concept of diffuse boundary over the western Mediterranean has been recently questioned in the Alboran basin, where geophysical evidence shows that a well-defined narrow plate boundary, which has absorbed up to about 20 km of Plio-Holocene contractional displacement, has already formed (Gómez de la Peña et al., 2022).

In the Atlantic Ocean (i.e., Gulf of Cadiz), the new boundary (B1 in Fig. 8) and the previous one (DeMets et al., 2010) mostly coincide as also suggested by the distribution and density of earthquakes (Table 1, Fig. 3). From the Gulf of Cadiz to the Gibraltar Arc, the old boundary instead stands at lower latitudes than our boundary. In this region, in fact, most earthquakes occur to the north of the old boundary, where we have redrawn the new one (Fig. 8). Kinematics of the new boundary is mostly compressive with right-lateral displacements in the Atlantic Ocean and the Gulf of Cadiz and right-lateral transcurrent close to the Gibraltar Arc.

Sector B2 of our boundary is identified in the western Rif system (Fig. 8) by several GNSS stations and focal mechanisms. This segment mostly coincides with an active NW-SE striking reverse fault (Table 1).

In the eastern Rif system, our boundary (B3 in Fig. 8) mostly follows the western Nekor Fault (Meghraoui et al., 1996) and shows a left lateral kinematics on E-W striking fault segments. This sector is also identified by a differential motion of the geodetic velocities at stations located across the boundary and by focal mechanisms (Table 1).

Following the new plate boundary toward the east, sectors B4 and B5 can be detected in the Gulf of Al Hoceima and the southern Alboran Sea (Fig. 8), along the Trougout Fault system, the southern Trans-Alboran shear zone (i.e., the Al-Idrissi fault segment; Gràcia et al., 2019) and the Alboran Ridge Fault System (Fig. 2). The Trougout Fault system is characterized by extensional and left-lateral kinematics on NNW-SSE striking faults, whereas the Trans-Alboran shear zone and the Alboran Ridge Fault system by reverse and left-lateral kinematics (see also Gómez de la Peña et al., 2022 and references therein). These segments are defined by GNSS stations and by a dense distribution of earthquakes and focal mechanisms (Table 1). In sectors B2, B3, B4 and B5, the old plate boundary is traced at latitudes lower than the new one (Fig. 8).

At the western edge of sector B5, a potential northward deviation of the new boundary with respect to the old one is observed, due to the abundance of evidence from GNSS data, earthquake distribution, focal mechanisms, and bathymetry (Table 1, Fig. 8). This segment partly coincides with the northern Trans-Alboran shear zone (Gràcia et al., 2019 and references therein). Two new segments (B6 and B7, Fig. 8) are described for the first time in this paper: one in the northern Alboran Sea and Eastern Betics areas and the other in the eastern Betics offshore region. The B6 segment mostly follows the northern Trans-Alboran shear zone (Gràcia et al., 2019 and references therein) and the Alhama de Murcia fault system (Masana et al., 2004 and references therein) (Fig. 2), whereas the B7 segment is aligned with morphological evidence in the eastern Betics offshore (e.g., https://www.emodnet-bathymetry.eu). The kinematics is reverse and left-lateral in sector B6 and right-lateral transpressive in sector B7.

In the Eastern Alboran Sea, we have identified a boundary segment (B8 in Fig. 8) that follows the transcurrent Yusuf fault system (Mauffret et al., 2007). This segment, which is mostly inferred from seismological data reported in Table 1 and is characterized by a right-lateral transpressive kinematics, mostly coincides with the previous boundary proposed by DeMets et al. (2010) (Fig. 8).

The longest segment (B9) is observed in the Algerian offshore (Fig. 8). We propose that such a boundary should be placed at the foot of the continental slope, based on morphological evidence of available bathymetry and pattern of geodetic velocities as well as crustal earthquake distribution and focal mechanisms (Table 1). Indeed, our boundary continues toward the east at higher latitudes with respect to the old boundary (Fig. 8). Our choice is driven by the base of the continental scarp, by morphological data (Fig. 8), by the location of the main thrust faults (Fig. 2), and by tectonic data from Strzerzynski et al. (2021), Klingelhoefer et al. (2022), and references therein. For this segment (B9), we suggest

Table 1
Label, location, kinematics and constraining observations of the nascent AF-EU plate boundary drawn in this study by using our geodetic (Table S5) and seismic (Tables S2, S3) datasets as well as by morpho-geo-structural data coming from the literature (Figs. 2, 8).

Label	Location	Kinematics	Constraining observations
B1	Gulf of Cadiz – Gibraltar Arc (−11.570°E, 35.884°N) (−5.996°E, 35.599°N)	Compressive with right lateral kinematics	– Earthquake distribution (see Table S2); – Focal mechanisms (Ids: FM_82, FM_114).
B2	Western Rif system (−5.996°E, 35.599°N) (−4.983°E, 34.659°N)	Compressive kinematics on NW-SE reverse faults	– GNSS data (TNIN, OUZS, CHEF, LAOU, TETN). – Active faults (Internal thrust). – Focal mechanisms (Ids: FM_63)
B3	Eastern Rif system (−4.983°E, 34.659°N) (−3.814°E, 34.933°N)	Left lateral kinematics on E-W faults	– GNSS data (KTMA, MSLA); – Active faults (western Nekor fault); – Focal mechanisms (Ids: FM_108, FM_109).
B4	Gulf of Al Hoceima (−3.814°E, 34.933°N) (−3.740°E, 35.550°N)	Extensional with left-lateral kinematics on NNW-SSE faults	– GNSS data (KTMA, BBFH, MDAR, MELI); – Earthquake distribution (see Table S2); – Focal mechanisms (Ids: FM_39, FM_40, FM_101, FM_102, FM_103, FM_104, FM_105, FM_106, FM_107, FM_186, FM_188, FM_194, FM_197, FM_200, FM_228); – Active faults (Trougout fault system).
B5	Southern Alboran sea (−3.740°E, 35.550°N) (−2.889°E, 36.181°N)	Reverse and left-lateral kinematics	– GNSS data (ALBO); – Earthquake distribution (see Table S2); – Focal mechanisms (Ids: FM_46, FM_83, FM_172, FM_183, M_184, FM_185, FM_187, FM_189, FM_190, FM_193, FM_195, FM_196, FM_198, FM_199); – Active faults (Southern trans-Alboran shear zone; Alboran Ridge fault system).
B6	Northern Alboran Sea – Eastern Betics (−2.889°E, 36.181°N) (−0.699°E, 38.207°N)	Reverse and left-lateral kinematics	– GNSS data (ABAN, MUR1, TORR, SALI, ALCA, CABO, CARG, MAJA, MAZA, GANU, PURI, MELL, TERC, ALHA, ESPU, MULA, AREZ, PUAS, HUOV, HUER, MOJA, CARB, RELL, ALME, CAAL); – Earthquake distribution (see Table S2); – Focal mechanisms (Ids: FM_1, FM_24, FM_38, FM_54, FM_57, FM_60, FM_69, FM_72, FM_115, FM_146, FM_147, FM_191); – Active faults (Northern trans-Alboran shear zone; Alhama de Murcia fault system).
B7	Eastern Betics offshore (−0.699°E, 38.207°N) (1.150°E, 37.837°N)	Right-lateral transpressive kinematics	– Earthquake distribution (see Table S2); – Morphological evidence from available bathymetry (https://www.emodnet-bathymetry.eu).
B8	Eastern Alboran Sea (−2.889°E, 36.181°N) (−1.083°E, 35.777°N)	Right-lateral transpressive kinematics	– Earthquake distribution (see Table S2); – Focal mechanisms (Ids: FM_58, FM_209); – Active faults (Yusuf fault system).
B9	Algerian offshore margin (−1.083°E, 35.777°N) (8.736°E, 37.601°N)	Compressive with right-lateral kinematics	– Earthquake distribution (see Table S2); – Focal mechanisms (Ids: FM_30, FM_43, FM_84, FM_85, FM_86, FM_87, FM_88, FM_89, FM_90, FM_91, FM_92, FM_93, FM_94, FM_95, FM_96, FM_97, FM_98, FM_99, FM_100, FM_119, FM_125, FM_132, FM_133, FM_151, FM_157, FM_163, FM_173, FM_215, FM_219, FM_225, FM_226); – Morphological evidence from available bathymetry (https://www.emodnet-bathymetry.eu); – Tectonic data from Strzerzynski et al. (2021), Klingelhoefer et al. (2022).
B10	Tunisian offshore margin (8.736°E, 37.601°N) (11.395°E, 38.496°N)	Compressive kinematics	– Scattered seismicity (see Table S2); – Active faults (e.g. Hatay fault; Camafort et al., 2022)
B11	Southern Tyrrhenian Sea (11.395°E, 38.496°N) (14.237°E, 38.648°N)	Compressive kinematics	– GNSS data (USIX, IACL); – Earthquake distribution (see Table S2); – Focal mechanisms (Ids: FM_48, FM_49, FM_50, FM_51, FM_53, FM_59, FM_73, FM_74, FM_75, FM_76, FM_77, FM_78, FM_137); – Morphological evidence from available bathymetry (https://www.emodnet-bathymetry.eu); – Tectonic data from Billi et al. (2011), Cuffaro et al. (2011).
B12	Western Aeolian Islands (14.237°E, 38.648°N) (14.783°E, 38.481°N)	Right-lateral kinematics with transpressive components	– GNSS data (IACL, IFIL); – Earthquake distribution (see Table S2); – Focal mechanisms (Ids: FM_13); – Active faults (Sisifo-Alicudi fault system).
B13	Southern Aeolian Islands – Northeastern Sicily (14.783°E, 38.481°N) (15.325°E, 37.813°N)	Right-lateral kinematics with transpressive and transtensive components	– GNSS data (LOSV, IVLT, IVUG, IVGP, TIND, PATT, MNOV, MCSR, TAOR); – Earthquake distribution (see Table S2); – Focal mechanisms (Ids: FM_56, FM_144, FM_148, FM_165, FM_166, FM_79, FM_80, FM_131); – Active faults (Aeolian-Tindari-Letojanni fault system).
B14	Ionian Sea (15.325°E, 37.813°N) (17.000°E, 35.703°N)	Compressive/transpressive kinematics	– Morphological evidence from available bathymetry (https://www.emodnet-bathymetry.eu); – Focal mechanisms (Ids: FM_81, FM_45, FM_213, FM_214); – Tectonic data from Polonia et al. (2016), Gutscher et al. (2017).

a compressive kinematics with an oblique right-lateral component as predicted by geodetic plate velocities and the block model results described in Bougrine et al. (2019). In the central part of sector B9, the new and old boundaries differ (Fig. 8), whereas moving eastward along the connection between the Algerian basin and the Tyrrhenian Sea (B9), the two boundaries mostly overlap (Fig. 8), both standing close to the location of a main thrust fault (Fig. 2).

To the south of Sardinia, only few data are available. Active shortening can be inferred from GNSS data between Sardinia and northern Tunisia-western Sicily (B10, Fig. 8), therefore suggesting the presence of tectonic structures that absorb the compressive deformation aseismically or with low-energy seismicity. This compressive segment should connect the north-dipping active thrusts in the Tyrrhenian margin with the south-dipping active ones in the Algerian margin. An alternative view could be that the deformation is diffusely distributed (aseismically or through low-magnitude earthquakes) over a number of small structures to the north of Tunisia (Camafort et al., 2022) and partly transferred northward in the Ligurian Sea (off Provence) where compressive earthquakes are known to occur frequently (Bigot-Cormier et al., 2004; Billi et al., 2011; Larroque et al., 2021).

To the south of Sardinia (B10), we have decided to redraw a new boundary passing at lower latitudes than the old boundary, following the scattered seismicity that occurs in this area (Table 1, Fig. 8) and the Hatay fault described by Camafort et al. (2022). As for the previous segment of the new plate boundary, no data are available to predict plate kinematics, so we suppose a compressive kinematics, as suggested by geodetic plate motion models (Fig. S3).

A well-defined and previously studied segment of the nascent AF-EU boundary can be placed in the southern Tyrrhenian Sea (B11, Fig. 8), along an E-W compressive belt passing north of Ustica Island, as inferred from GNSS data, earthquake distribution, focal mechanisms, morphological evidence (i.e., bathymetry), and tectonic data from Billi et al. (2006, 2007) and Cuffaro et al. (2011). This segment stands at latitudes higher than the previous one. In our opinion, the E-W-trending compressive belt passing north of Ustica Island is a better candidate than the old one (located a few km toward the south; Fig. 8d) to represent the AF-EU boundary. Indeed, since the USIX station (Ustica Island) velocity is slower than those in northern Sicily (Fig. 8), we suggest that this difference can be associated to strain accommodation of active faults located in the southern Tyrrhenian Sea (Billi et al., 2007; Cuffaro et al., 2011).

This last sector (B11) is directly linked with the next B12 and B13 sectors in the Western Aeolian Islands and Southern Aeolian Islands-Northeastern Sicily areas (Fig. 8), along the Sisifo-Alicudi fault system and the Aeolian-Tindari-Letojanni fault system, respectively (Fig. 2). These two sectors can be easily traced by GNSS data, earthquake distribution, and focal mechanisms (Table 1). A right-lateral kinematics with transpressive components and a right-lateral one with transpressive and transtensive components are observed in sectors B12 and B13, respectively. In these sectors, the new boundary stands at latitudes lower than the previous one (Fig. 8).

Finally, in the Ionian Sea (B14 in Fig. 8), the new boundary follows the evidence provided by morphological evidence from available bathymetry, focal mechanisms and tectonic data from Polonia et al. (2016), Gutscher et al. (2017), and Sgroi et al. (2021) with a compressive to oblique kinematics. Our boundary stands at lower latitudes than the previously drawn one (Fig. 8).

4.3. Tectonic implications

To infer some broad tectonic implications, we use the angular relationships between main seismic and geodetic axes and the strike of the nascent AF-EU boundary (Figs. 9a–9f). Fig. 9a shows that the horizontal components of the compressive seismic stress (from focal mechanisms, Fig. 6) and geodetic strain (Fig. 7b) are mostly coincident all over the entire nascent boundary, hence supporting each other.

Our angular analyses show also that the general motion of AF with respect to EU (Altamimi et al., 2017) locally forms angles with the trend of the nascent boundary that are not 90° or so as expected along a convergent margin, but are highly variable with frequent values at about 78° and 13° (Figs. 9a and 9d). This apparently odd angular pattern is mirrored by the angles locally formed by the trend of the nascent boundary and the horizontal components of the compressive seismic stress and geodetic strain (Figs. 9b and 9c, respectively). These angles are indeed mostly included between 45° and 78°. These angular relationships (Figs. 9b, 9c, and 9d) show the high immaturity (sensu Lallemand and Arcay, 2021) of the nascent boundary that is probably forming through the reuse or reactivation of inherited structures (e.g., Benabdellouahed et al., 2017; Gómez de la Peña et al., 2018, 2022) obliquely oriented with respect to the main driving forces. Figs. 9a and 9d show also that, locally, the nascent boundary and the general motion of AF with respect to EU are nearly parallel (they usually form an angle $\leq 15°$). This evidence shows the occurrence of strike-slip zones of displacement transfer (i.e., future transform zones?) linking segments characterized by contractional displacement. Examples are in the Ionian Sea, Alboran Sea, and Gibraltar area, suggesting an additional tectonic complexity of the nascent AF-EU boundary (Figs. 9a and 9g). Moreover, Figs. 9a, 9e, and 9f show that, locally, angles included between about 22° and 45° exist between the general motion of AF with respect to EU and the horizontal components of the compressive seismic stress and geodetic strain-rates. Such an evidence – although we are aware that the predicted AF-EU general motion from plate kinematic models correspond to average smoothed plate velocities (Fig. S3) – apparently suggests a non-correlation or a limited one between the nascent boundary and regional plate tectonics. The reason for this apparent angular discrepancy is, as explained above, in the local accommodation of converging motions between AF and EU along variably-oriented pre-existing weak structures. The reason, in other words, is in the immaturity of the nascent boundary (Lallemand and Arcay, 2021). To this end, it is also relevant to mention that, in the wide statistics of Lallemand and Arcay (2021), about 55% of the studied cases is characterized by an oblique direction of convergence at subduction initiation zones and only about 25% is characterized by a normal direction. Figs. 9b and 9c show that our study case is consistent with the majority of cases (including the western Mediterranean) studied by Lallemand and Arcay (2021). It is, however, also true that the present average convergence rate across the western Mediterranean is about 5 mm/yr, which is a velocity considered highly unsuccessful by Lallemand and Arcay (2021) to arrive at a mature subduction zone in the future. It would take ten times as much speed to develop a self-sustained subduction zone. Nonetheless, we are aware that back-arc basins of the past were often compressed, closed, and included in suture zones between continents. Examples of ancient systems include the Newfoundland (Cawood and Suhr, 1992) and Norwegian (Slagstad and Kirkland, 2018) Caledonides, Black Sea (Munteanu et al., 2011), Patagonian Andes (Muller et al., 2021), and Eastern Tianshan (Jiang et al., 2017). In this sense, the present setting of the Mediterranean is an optimal laboratory where studying, understanding, and even envisaging subduction inception and complex suture zones. Some themes of complexity (partly mentioned above) are, for instance: (1) the irregular shape of basins to be presumably subducted that would form irregular or arched subduction zones, rigid-block rotations about vertical axes, or oblique subductions; (2) the different degrees of oceanization in the Liguro-Provençal and Tyrrhenian basins that would generate lateral differential tectonic regimes along the suture zones forcibly separated by transfer of transform zones; (3) the occurrence of the Corsica-Sardinia block (transversely to the suture zone) that would opposite the closure of the western Mediterranean or at least separate two diverse domains (Liguro-Provençal and Tyrrhenian) of plate convergence; and (4) the occurrence of compressional tectonics along both margins of the Liguro-Provençal basin (Algeria to the

south and Betics and Provence to the north) that would generate a doubly-vergent suture-subduction zone.

To start unraveling some of the above mentioned themes of complexity for the future tectonics of the western Mediterranean, upon the assumption of a future northward tectonic vergence (i.e., Eurasian foreland), in Fig. 9g, we suggest the occurrence of nascent salients and recesses, which are, respectively, convex-to-the-foreland and concave-to-the-foreland curves (in map view) of fold-thrust belts. We identify, in particular, the Tyrrhenian, Algerian, and Betic salients, the Oran and Fès recesses, and the Ionian, Trans-Alboran, and Gibraltar transfer zones. These latter three zones connect salients and recesses through strike-slip displacements. Moreover, the Gibraltar transfer zone joins toward the west with an additional potential salient (i.e., the Goringe salient located outside Fig. 9g; see Zitellini et al., 2009), where future subduction of the Atlantic lithosphere toward southeast has been hypothesized (Duarte et al., 2013).

In our tectonic model of Fig. 9g, there are at least three questionable structures. The first one is the Betic salient, which would imply a southward underthrusting or even subduction of the Iberian continental block. This process is mechanically unlikely and hence we recognize that the term salient for the convex-to-the-north boundary in the Betics is highly questionable. The second odd structure is the boundary segment located to the south of Sardinia. As explained above, this segment seems faintly active and part of the convergent displacement may be transferred off Provence. The presence of the rigid Corsica-Sardinia block and of converging structures at the opposite sides of the Mediterranean basin (i.e., as far as 600 km) make this setting too complex (doubly-vergent suture?) for suitable predictions. The third structure is the south Tyrrhenian, where active thrusting presumably with a southward vergence (Billi et al., 2007) and the limited (or null) oceanization of the Tyrrhenian basin makes its future subduction unlikely. Therefore, also in this case, the term Tyrrhenian salient may be questionable. In contrast, the Algerian offshore hosts a long segment of the boundary characterized by high seismic rate and actual northward vergence that would suggest this area being the first nucleus of subduction initiation in the western Mediterranean (e.g., Déverchère et al., 2005).

5. Conclusions

New earthquake and GNSS data together with pre-existing tectonic data have guided us in drawing a nascent plate boundary between the converging Africa and Eurasia plates in the western Mediterranean back-arc basins. The new boundary connects the still active subductions – occurring toward the east in the Ionian area and toward the west in Alboran and Atlantic basins – through compressional segments and transfer zones inverting and segmenting the Tyrrhenian, Liguro-Provencal, and Alboran back-arc basins. In the assumption that Eurasia becomes the future foreland, potential salients (Tyrrhenian, Algerian, and Betic), recesses (Oran and Fès), and transfer zones (Ionian, Trans-Alboran, and Gibraltar) connecting salients and recesses are identified along the nascent boundary. These features originated at least in part from inherited structures including the architecture of the inverted sedimentary basins and an originally nonlinear continental margin. This nascent pattern is relevant for understanding the origin and evolution of weaving fold-thrust belts and, vice versa, to envisage the future evolution of the nascent boundary in the western Mediterranean. All the above-discussed deformation features provide clear evidence for a substantial fragmentation of the western Mediterranean tectonic boundary between Africa and Eurasia, associated with basins into independent crustal tectonic blocks, which are passively involved within the main Africa–Eurasia convergence.

A series of tectonic implications can be drawn from this study. The seismic and geodetic data across the nascent boundary are consistent, hence mutually supporting. The nascent boundary is very sinuous and irregular over the western Mediterranean, consistently with its infant or immature stage of subduction initiation zones (sensu Lallemand and Arcay, 2021) that are influenced by numerous weak inherited structures. The immature stage and the role of inherited structures would explain not only the irregular geometry of the nascent boundary but also the apparent discrepancies between the general motion of Africa with respect to Europe and the local contractional/compressive directions along the nascent boundary, as deduced from geodetic and seismic data. Moreover, it is demonstrated that subduction initiations are usually characterized by oblique motions across the nascent boundaries, and this is also the case for the western Mediterranean, where, however, the average convergence rate (about 5 mm/yr) seems at present too small to successfully arrive at a mature subduction zone in the future (Lallemand and Arcay, 2021).

CRediT authorship contribution statement

A. Billi: research coordination, conceptualization, writing, review and editing. **M. Cuffaro**: conceptualization, formal analysis, writing, review and editing. **B. Orecchio**: formal analysis, conceptualization, writing, review and editing. **M. Palano**: research coordination, formal analysis, conceptualization, writing, review and editing. **D. Presti**: research coordination, formal analysis, conceptualization, writing, review and editing. **C. Totaro**: formal analysis, conceptualization, writing, review and editing.

Declaration of competing interest

The authors declare that they have no known competing financial interests or personal relationships that could have appeared to influence the work reported in this paper.

Data availability

Data will be made available on request.

Acknowledgements

We warmly thank R. Govers, L. Jolivet, and H. Thybo for their constructive suggestions. We acknowledge no funding for this study except the ordinary institutional ones (i.e., from authors' institutions).

Appendix A. Supplementary material

Supplementary material related to this article can be found online at https://doi.org/10.1016/j.epsl.2022.117906.

References

Altamimi, Z., Métivier, L., Rebischung, P., Rouby, H., Collilieux, X., 2017. ITRF2014 plate motion model. Geophys. J. Int. 209 (3), 1906–1912. https://doi.org/10.1093/gji/ggx136.

Arnold, R., Townend, J., 2007. A Bayesian approach to estimating tectonic stress from seismological data. Geophys. J. Int. 170, 1336–1356. https://doi.org/10.1111/j.1365-246X.2007.03485.x.

Auzemery, A., Willingshofer, E., Sokoutis, D., Brun, J.P., Cloetingh, S.A., 2021. Passive margin inversion controlled by stability of the mantle lithosphere. Tectonophysics 817, 229042. https://doi.org/10.1016/j.tecto.2021.229042.

Benabdellouahed, M., Klingelhoefer, F., Gutscher, M.A., Rabineau, M., Biari, Y., Hafid, M., Duarte, J.C., Schnabel, M., Baltzerh, A., Pedojai, K., Le Roy, P., Reichert, C., Sahabi, M., 2017. Recent uplift of the Atlantic Atlas (offshore West Morocco): tectonic arch and submarine terraces. Tectonophysics 706, 46–58. https://doi.org/10.1016/j.tecto.2017.03.024.

Bigot-Cormier, F., Sage, F., Sosson, M., Déverchère, J., Ferrandini, M., Guennoc, P., Popoff, M., Stéphan, J.F., 2004. Déformations pliocenes de la marge nord-Ligure (France): les conséquences d'un chevauchement crustal sud-alpin. Bull. Soc. Géol. Fr. 175 (2), 197–211.

Billi, A., Barberi, G., Faccenna, C., Neri, G., Pepe, F., Sulli, A., 2006. Tectonics and seismicity of the Tindari Fault System, southern Italy: crustal deformations at the transition between ongoing contractional and extensional domains located above the edge of a subducting slab. Tectonics 25 (2). https://doi.org/10.1029/2004TC001763.

Billi, A., Faccenna, C., Bellier, O., Minelli, L., Neri, G., Piromallo, C., Presti, D., Scrocca, D., Serpelloni, E., 2011. Recent tectonic reorganization of the Nubia-Eurasia convergent boundary heading for the closure of the western Mediterranean. Bull. Soc. Géol. Fr. 182 (4), 279–303. https://doi.org/10.2113/gssgfbull.182.4.279.

Billi, A., Presti, D., Faccenna, C., Neri, G., Orecchio, B., 2007. Seismotectonics of the Nubia plate compressive margin in the south Tyrrhenian region, Italy: clues for subduction inception. J. Geophys. Res., Solid Earth 112 (B8). https://doi.org/10.1029/2006JB004837.

Bird, P., 2003. An updated digital model of plate boundaries. Geochem. Geophys. Geosyst. 4 (3). https://doi.org/10.1029/2001GC000252.

Bounif, A., Dorbath, C., Ayadi, A., Meghraoui, M., Beldjoudi, H., Laouami, N., Frogneux, M., Slimani, A., Alasset, P.J., Kharroubi, A., Ousadou, F., Chikh, M., Harbi, A., Larbes, S., Maouche, S., 2004. The 21 May 2003 Zemmouri (Algeria) earthquake Mw 6.8: relocation and aftershock sequence analysis. Geophys. Res. Lett. 31 (19). https://doi.org/10.1029/2004GL020586.

Buforn, E., López-Sánchez, C., Lozano, L., Martínez-Solares, J.M., Cesca, S., Oliveira, C.S., Udías, A., 2020. Re-evaluation of seismic intensities and relocation of 1969 Saint Vincent Cape seismic sequence: a comparison with the 1755 Lisbon earthquake. Pure Appl. Geophys. 177 (4), 1781–1800. https://doi.org/10.1007/s00024-019-02336-8.

Bougrine, A., Yelles-Chaouche, A.K., Calais, E., 2019. Active deformation in Algeria from continuous GPS measurements. Geophys. J. Int. 217 (1), 572–588. https://doi.org/10.1093/gji/ggz035.

Carminati, E., Wortel, M.J.R., Spakman, W., Sabadini, R., 1998. The role of slab detachment processes in the opening of the western–central Mediterranean basins: some geological and geophysical evidence. Earth Planet. Sci. Lett. 160 (3–4), 651–665. https://doi.org/10.1016/S0012-821X(98)00118-6.

Cawood, P.A., Suhr, G., 1992. Generation and obduction of ophiolites: constraints from the Bay of Islands Complex, western Newfoundland. Tectonics 11 (4), 884–897. https://doi.org/10.1029/92TC00471.

Camafort, M., Ranero, C.R., Gràcia, E., 2022. Active tectonics of the North Tunisian continental margin. Tectonics 41, e2021TC007110. https://doi.org/10.1029/2021TC007110.

Cuffaro, M., Riguzzi, F., Scrocca, D., Doglioni, C., 2011. Coexisting tectonic settings: the example of the southern Tyrrhenian Sea. Int. J. Earth Sci. 100 (3), 1915–1924. https://doi.org/10.1007/s00531-010-0625-z.

DeMets, C., Gordon, R.G., Argus, D.F., Stein, S., 1990. Current plate motions. Geophys. J. Int. 101, 425–478. https://doi.org/10.1111/j.1365-246X.1990.tb06579.x.

DeMets, C., Gordon, R.G., Argus, D.F., 2010. Geologically current plate motions. Geophys. J. Int. 181, 1–80. https://doi.org/10.1111/j.1365-246X.2009.04491.x.

Déverchère, J., Yelles, K., Domzig, A., Mercier de Lépinay, B., Bouillin, J.-P., Gaullier, V., Bracène, R., Calais, E., Savoye, B., Kherroubi, A., Le Roy, P., Pauch, H., Dan, G., 2005. Active thrust faulting offshore Boumerdes, Algeria, and its relations to the 2003 Mw 6.9 earthquake. Geophys. Res. Lett. 32, L04311. https://doi.org/10.1029/2004GL021646.

Devoti, R., D'Agostino, N., Serpelloni, E., Pietrantonio, G., Riguzzi, F., Avallone, A., Cavaliere, A., Cheloni, D., Cecere, G., D'Ambrosio, C., Falco, L., Selvaggi, G., Métois, M., Esposito, A., Sepe, V., Galvani, A., Anzidei, M., 2017. A combined velocity field of the Mediterranean region. Ann. Geophys. 60 (2), S0215. https://doi.org/10.4401/ag-7059.

Duarte, J.C., Rosas, F.M., Terrinha, P., Schellart, W.P., Boutelier, D., Gutscher, M.A., Ribeiro, A., 2013. Are subduction zones invading the Atlantic? Evidence from the southwest Iberia margin. Geology 41 (8), 839–842. https://doi.org/10.1130/G34100.1.

Echeverria, A., Khazaradze, G., Asensio, E., Gárate, J., Dávila, J.M., Suriñach, E., 2013. Crustal deformation in eastern Betics from CuaTeNeo GPS network. Tectonophysics 608, 600–612. https://doi.org/10.1016/j.tecto.2013.08.020.

Faccenna, C., Becker, T.W., Auer, L., Billi, A., Boschi, L., Brun, J.-P., Capitanio, F.A., Funiciello, F., Horvàth, F., Jolivet, L., Piromallo, C., Royden, L., Rossetti, F., Serpelloni, E., 2014. Mantle dynamics in the Mediterranean. Rev. Geophys. 52, 283–332. https://doi.org/10.1002/2013RG000444.

Gómez de la Peña, L., Ranero, C.R., Gràcia, E., 2018. The crustal domains of the Alboran Basin (western Mediterranean). Tectonics 37, 3352–3377. https://doi.org/10.1029/2017TC004946.

Gómez de la Peña, L., Ranero, C.R., Gràcia, E., Booth-Rea, G., Azañón, J.M., Tinivella, U., Yelles-Chaouche, A., 2022. Evidence for a developing plate boundary in the western Mediterranean. Nat. Commun. 13, 4786. https://doi.org/10.1038/s41467-022-31895-z.

Gràcia, E., Grevemeyer, I., Bartolomé, R., Perea, H., Martínez-Loriente, S., Gómez De La Peña, L., Villaseñor, A., Klinger, Y., Lo Iacono, C., Diez, S., Calahorrano, A., Camafort, M., Costa, S., d'Acremont, E., Rabaute, A., Ranero, C.R., 2019. Earthquake crisis unveils the growth of an incipient continental fault system. Nat. Commun. 10 (1), 1–12. https://doi.org/10.1038/s41467-019-11064-5.

Gutscher, M., Kopp, H., Krastel, S., Bohrmann, G., Garlane, T., Zaragosi, S., Klaucke, I., Wintersteller, P., Loubrieu, B., Le Faou, Y., San Pedro, L., Dominguez, S., Rovere, M., Mercier de Lepinay, B., Ranero, C., Sallares, V., 2017. Active tectonics of the Calabrian subduction revealed by new multi-beam bathymetric data and high resolution seismic profiles in the Ionian Sea (Central Mediterranean). Earth Planet. Sci. Lett. 461, 61–72. https://doi.org/10.1016/j.epsl.2016.12.020.

Haidar, S., Déverchère, J., Graindorge, D., Arab, M., Medaouri, M., Klingelhoefer, F., 2022. Back-arc dynamics controlled by slab rollback and tearing: a reappraisal of seafloor spreading and kinematic evolution of the Eastern Algero-Balearic Basin (western Mediterranean) in the Middle-Late Miocene. Tectonics 41 (2), e2021TC006877. https://doi.org/10.1029/2021TC006877.

Jiang, H., Han, J., Chen, H., Zheng, Y., Lu, W., Deng, G., Tan, Z., 2017. Intracontinental back-arc basin inversion and Late Carboniferous magmatism in Eastern Tianshan, NW China: constraints from the Shaquanzi magmatic suite. Geosci. Front. 8 (6), 1447–1467. https://doi.org/10.1016/j.gsf.2017.01.008.

Jiménez-Munt, I., Sabadini, R., Gardi, A., Bianco, G., 2003. Active deformation in the Mediterranean from Gibraltar to Anatolia inferred from numerical modeling and geodetic and seismological data. J. Geophys. Res., Solid Earth 108 (B1), ETG-2. https://doi.org/10.1029/2001JB001544.

Jolivet, L., Baudin, T., Calassou, S., Chevrot, S., Ford, M., Issautier, B., Lasseur, E., Masini, E., Manatschal, G., Mouthereau, F., Thinon, I., Vidal, O., 2021. Geodynamic evolution of a wide plate boundary in the Western Mediterranean, near-field versus far-field interactions. BSGF Earth Sci. Bull. 192 (1), 48. https://doi.org/10.1051/bsgf/2021043.

Jolivet, L., Faccenna, C., 2000. Mediterranean extension and the Africa–Eurasia collision. Tectonics 19 (6), 1095–1106. https://doi.org/10.1029/2000TC900018.

Kastens, K.A., Mascle, J., 1990. The geological evolution of the Tyrrhenian sea: an introduction to the scientific results of ODP Leg 107. Proc. Ocean Drill. Program Sci. Results 107, 3–26. https://doi.org/10.2973/odp.proc.sr.107.187.1990.

Kherroubi, A., Déverchère, J., Yelles, A., De Lépinay, B.M., Domzig, A., Cattaneo, A., Bracène, R., Gaullier, V., Graindorge, D., 2009. Recent and active deformation pattern off the easternmost Algerian margin, Western Mediterranean Sea: new evidence for contractional tectonic reactivation. Mar. Geol. 261 (1–4), 17–32. https://doi.org/10.1016/j.margeo.2008.05.016.

Klingelhoefer, F., Déverchère, J., Graindorge, D., Aïdi, C., Badji, R., Bouyahiaoui, B., Leprêtre, A., Mihoubi, A., Beslier, M.-O., Charvis, P., Schnurle, P., Sage, F., Medaouri, M., Arab, M., Bracene, R., Yelles-Chaouche, A., Badsi, M., Galvé, A., Géli, L., 2022. Formation, segmentation and deep crustal structure variations along the Algerian margin from the SPIRAL seismic experiment. J. Afr. Earth Sci. 104. https://doi.org/10.1016/j.jafrearsci.2021.104433.

Kreemer, C., Blewitt, G., Klein, E.C., 2014. A geodetic plate motion and Global Strain Rate Model. Geochem. Geophys. Geosyst. 15 (10), 3849–3889. https://doi.org/10.1002/2014GC005407.

Lallemand, S., Arcay, D., 2021. Subduction initiation from the earliest stages to self-sustained subduction: insights from the analysis of 70 Cenozoic sites. Earth-Sci. Rev. 103779. https://doi.org/10.1016/j.earscirev.2021.103779.

Larroque, C., Baize, S., Albaric, J., Jomard, H., Trévisan, J., Godano, M., Cushing, M., Deschamps, A., Sue, C., Delouis, B., Potin, B., Courboulex, F., Régnier, M., Rivet, D., Brunel, D., Chèze, J., Martin, X., Maron, C., Peix, F., 2021. Seismotectonics of southeast France: from the Jura mountains to Corsica. C. R. Géosci. 353 (S1), 105–151. https://doi.org/10.5802/crgeos.69.

Leffondré, P., Déverchère, J., Medaouri, M., Klingelhoefer, F., Graindorge, D., Arab, M., 2021. Ongoing inversion of a passive margin: spatial variability of strain markers along the Algerian margin and basin (Mediterranean Sea) and seismotectonic implications. Front. Earth Sci. 9c, 674584. https://doi.org/10.3389/feart.2021.674584.

Masana, E., Martínez-Díaz, J.J., Hernández-Enrile, J.L., Santanach, P., 2004. The Alhama de Murcia fault (SE Spain), a seismogenic fault in a diffuse plate boundary: seismotectonic implications for the Ibero-Magrebian region. J. Geophys. Res., Solid Earth 109 (B1). https://doi.org/10.1029/2002JB002359.

Mauffret, A., Ammar, A., Gorini, C., Jabour, H., 2007. The Alboran Sea (Western Mediterranean) revisited with a view from the Moroccan Margin. Terra Nova 19, 195–203. https://doi.org/10.1111/j.1365-3121.2007.00734.x.

McKenzie, D., 1972. Active tectonics of the Mediterranean region. Geophys. J. Int. 30 (2), 109–185. https://doi.org/10.1111/j.1365-246X.1972.tb02351.x.

Meghraoui, M., Maouche, S., Chemaa, B., Cakir, Z., Aoudia, A., Harbi, A., Alasset, P.-J., Ayadi, A., Bouhadad, Y., Benhamouda, F., 2004. Coastal uplift and thrust faulting associated with the Mw = 6.8 Zemmouri (Algeria) earthquake of 21 May, 2003. Geophys. Res. Lett. 31 (19). https://doi.org/10.1029/2004GL020466.

Meghraoui, M., Morel, J.L., Andrieux, J., Dahmani, M., 1996. Pliocene and quaternary tectonics of the Tell-Rif mountains and Alboran sea, a complex zone of continent-continent convergence. Bull. Soc. Géol. Fr. 167, 141–157.

Muller, V.A., Calderón, M., Fosdick, J.C., Ghiglione, M.C., Cury, L.F., Massonne, H.J., Fanning, C.M., Warren, C.J., de Arellano, C.R., Sternai, P., 2021. The closure of the Rocas Verdes Basin and early tectono-metamorphic evolution of the Magallanes Fold-and-Thrust Belt, southern Patagonian Andes (52–54° S). Tectonophysics 798, 228686. https://doi.org/10.1016/j.tecto.2020.228686.

Müller, R.D., Zahirovic, S., Williams, S.E., Cannon, J., Seton, M., Bower, D.J., Tetley, M.G., Heine, C., Le Breton, E., Liu, S., Russell, S.H.J., Yang, T., Leonard, J., Gur-

nis, M., 2019. A global plate model including lithospheric deformation along major rifts and orogens since the Triassic. Tectonics 38. https://doi.org/10.1029/2018TC005462.

Munteanu, I., Matenco, L., Dinu, C., Cloetingh, S., 2011. Kinematics of back-arc inversion of the Western Black Sea Basin. Tectonics 30 (5). https://doi.org/10.1029/2011TC002865.

Nijholt, N., Govers, R., Wortel, R., 2018. On the forces that drive and resist deformation of the south-central Mediterranean: a mechanical model study. Geophys. J. Int. 214 (2), 876–894. https://doi.org/10.1093/gji/ggy144.

Nocquet, J.M., 2012. Present-day kinematics of the Mediterranean: a comprehensive overview of GPS results. Tectonophysics 579, 220–242. https://doi.org/10.1016/j.tecto.2012.03.037.

Okal, E.A., Synolakis, C.E., 2008. Far-field tsunami hazard from mega-thrust earthquakes in the Indian Ocean. Geophys. J. Int. 172, 995–1015. https://doi.org/10.1111/j.1365-246X.2007.03674.x.

Orecchio, B., Scolaro, S., Batlló, J., Neri, G., Presti, D., Stich, D., Totaro, C., 2021. New results for the 1968 Belice, South Italy, seismic sequence: solving the long-lasting ambiguity on causative source. Seismol. Res. Lett. 92 (4), 2364–2381. https://doi.org/10.1785/0220200277.

Ousadou, F., Bezzeghoud, M., 2019. Seismicity of the Algerian Tell Atlas and the impacts of major earthquakes. In: The Geology of the Arab World—An Overview. Springer, Cham, pp. 401–426.

Palano, M., Ferranti, L., Monaco, C., Mattia, M., Aloisi, M., Bruno, V., Cannavò, F., Siligato, G., 2012. GPS velocity and strain fields in Sicily and southern Calabria, Italy: updated geodetic constraints on tectonic block interaction in the central Mediterranean. J. Geophys. Res., Solid Earth 117 (B7). https://doi.org/10.1029/2012JB009254.

Palano, M., González, P.J., Fernández, J., 2015. The diffuse plate boundary of Nubia and Iberia in the western Mediterranean: crustal deformation evidence for viscous coupling and fragmented lithosphere. Earth Planet. Sci. Lett. 430, 439–447. https://doi.org/10.1016/j.epsl.2015.08.040.

Polonia, A., Torelli, L., Artoni, A., Carlini, M., Faccenna, C., Ferranti, L., Gasperini, L., Govers, R., Klaeschen, D., Monaco, C., Neri, G., Nijholt, N., Orecchio, B., Wortel, R., 2016. The Ionian and Alfeo–Etna fault zones: new segments of an evolving plate boundary in the central Mediterranean Sea? Tectonophysics 675, 69–90. https://doi.org/10.1016/j.tecto.2016.03.016.

Presti, D., Billi, A., Orecchio, B., Totaro, C., Faccenna, C., Neri, G., 2013. Earthquake focal mechanisms, seismogenic stress, and seismotectonics of the Calabrian Arc, Italy. Tectonophysics 602, 153–175. https://doi.org/10.1016/j.tecto.2013.01.030.

Royden, L., Faccenna, C., 2018. Subduction orogeny and the Late Cenozoic evolution of the Mediterranean arcs. Annu. Rev. Earth Planet. Sci. 46, 261–289. https://doi.org/10.1146/annurev-earth-060115-012419.

Sartori, R., 1990. The main results of ODP Leg 107 in the frame of Neogene to recent geology of perityrrhenian areas. In: Kastens, K.A., et al. (Eds.), Proc. ODP Sci. Res., vol. 107. Ocean Drilling Program, College Station, Tex., pp. 715–730.

Serpelloni, E., Vannucci, G., Pondrelli, S., Argnani, A., Casula, G., Anzidei, M., Baldi, P., Gasperini, P., 2007. Kinematics of the Western Africa–Eurasia plate boundary from focal mechanisms and GPS data. Geophys. J. Int. 169 (3), 1180–1200. https://doi.org/10.1111/j.1365-246X.2007.03367.x.

Sgroi, T., Polonia, A., Barberi, G., Billi, A., Gasperini, L., 2021. New seismological data from the Calabrian arc reveal arc-orthogonal extension across the subduction zone. Sci. Rep. 11, 473. https://doi.org/10.1038/s41598-020-79719-8.

Shen, Z.K., Wang, M., Zeng, Y., Wang, F., 2015. Optimal interpolation of spatially discretized geodetic data. Bull. Seismol. Soc. Am. 105 (4), 2117–2127. https://doi.org/10.1785/0120140247.

Slagstad, T., Kirkland, C.L., 2018. Timing of collision initiation and location of the Scandian orogenic suture in the Scandinavian Caledonides. Terra Nova 30 (3), 179–188. https://doi.org/10.1111/ter.12324.

Soumaya, A., Ben Ayed, N., Rajabi, M., Meghraoui, M., Delvaux, D., Kadri, A., Ziegler, M., Maouche, S., Braham, A., 2018. Active faulting geometry and stress pattern near complex strike-slip systems along the Maghreb Region: constraints on active convergence in the Western Mediterranean. Tectonics 37 (9), 3148–3173. https://doi.org/10.1029/2018TC004983.

Strzerzynski, P., Dominguez, S., Boudiaf, A., Déverchère, J., 2021. Tectonic inversion and geomorphic evolution of the Algerian margin since Messinian times: insights from new onshore/offshore analog modeling experiments. Tectonics 40, e2020TC006369. https://doi.org/10.1029/2020TC006369.

Thorwart, M., Dannowski, A., Grevemeyer, I., Lange, D., Kopp, H., Petersen, F., Crawford, W.C., Paul, A., AlpArray Working Group, 2021. Basin inversion: reactivated rift structures in the central Ligurian Sea revealed using ocean bottom seismometers. Solid Earth 12 (11), 2553–2571. https://doi.org/10.5194/se-12-2553-2021.

van Hinsbergen, D.J., Torsvik, T.H., Schmid, S.M., Maţenco, L.C., Maffione, M., Vissers, R.L., Gürer, D., Spakman, W., 2020. Orogenic architecture of the Mediterranean region and kinematic reconstruction of its tectonic evolution since the Triassic. Gondwana Res. 81, 79–229. https://doi.org/10.1016/j.gr.2019.07.009.

Yelles, A., Domzig, A., Déverchère, J., Bracène, R., de Lépinay, B.M., Strzerzynski, P., Bertrand, G., Boudiaf, A., Winter, T., Kherroubi, A., Le Roy, P., Djellit, H., 2009. Plio-Quaternary reactivation of the Neogene margin off NW Algiers, Algeria: the Khayr al Din bank. Tectonophysics 475 (1), 98–116. https://doi.org/10.1016/j.tecto.2008.11.030.

Yelles-Chaouche, A., Kherroubi, A., Beldjoudi, H., 2017. The large Algerian earthquakes (267 AD-2017). Fís. Tierra 29, 159. https://doi.org/10.5209/FITE.57617.

Wortel, M.J.R., Spakman, W., 2000. Subduction and slab detachment in the Mediterranean Carpathian region. Science 290, 1910–1917. https://doi.org/10.1126/science.290.5498.1910.

Zitellini, N., Gràcia, E., Matias, L., Terrinha, P., Abreu, M.A., DeAlteriis, G., Henriet, J.P., Dañobeitia, J.J., Masson, D.G., Mulder, T., Ramella, R., Somoza, L., Diez, S., 2009. The quest for the Africa–Eurasia plate boundary west of the Strait of Gibraltar. Earth Planet. Sci. Lett. 280, 13–50. https://doi.org/10.1016/j.epsl.2008.12.005.